LU TP 11-14
arXiv:1103.5945 [hep-ph]
Revised September 2011

A new global fit of the L_i^r at next-to-next-to-leading order in Chiral Perturbation Theory

Johan Bijnens and Ilaria Jemos

Department of Astronomy and Theoretical Physics, Lund University,
Sölvegatan 14A, SE 223-62 Lund, Sweden

Abstract

A new fit is done to obtain numerical values for the order p^4 low-energy-constants L_i^r in Chiral Perturbation Theory. This includes both new data and new calculated observables. We take into account masses, decay constants, $K_{\ell 4}$, $\pi\pi$ and πK scattering lengths and slopes and the slope of the pion scalar formfactor. We compare in detail where the changes w.r.t. to the 10 year old "fit 10" come from. We discuss several scenarios for estimating the order p^6 constants C_i^r and search for possible values of them that provide a good convergence for the ChPT series. We present two such sets. One big change is that the fits do not have the expected behaviour in the limit of large N_c as well as before.

1 Introduction

Since its very beginning Chiral Perturbation Theory (ChPT)[1, 2, 3], the effective field theory of QCD at low energies, has been successful in the description of several hadronic observables. Unfortunately when one tries to perform loop calculations to improve the precision of the predictions, one faces a problem. The couplings appearing in the $\mathcal{L}_4$ Lagrangian are many, i.e. 10, and they must be determined from phenomenology. One of the first determinations of such couplings was done already in [3]. There most of the next-to-leading order (NLO) couplings were inferred both from phenomenology and from considerations lead by large N_c estimates (where N_c is the number of colours).

Considering such good results it is important to decide whether ChPT is a suitable theory to achieve precise determinations of the hadronic observables. It urged then to carry on a program and perform next-to-next-to-leading order (NNLO) calculations [4]. In the last 10 years many two-loop calculations in three-flavour ChPT have been done, see [5] for a review.

Notice however that going to higher orders raises a serious issue: the number of the unknown couplings increases rapidly. If on the one side adding loop diagrams should allow us to include better corrections and improve our descriptions, on the other side, many unknown parameters contribute and this seriously threatens the predictivity of the theory. Furthermore without knowing the values of such constants the convergence of the chiral expansions are difficult to test, although feasible with the method described in [6].

The two-loop expressions now available can be used to perform a new global fit at NNLO of some of the next-to-leading-order (NLO) low-energy-constants (LECs) into the game, the L_i^r. A first attempt was done [7] when some experimental information was available for the $K_{\ell 4}$ decay and by estimating the NNLO contributions using dispersive analysis. The fit was refined later on, when the full NNLO calculation for this process was performed [8, 9]. After that many other observables have been calculated at NNLO and many of them are also better known experimentally. Therefore the time has come to perform a new fit of the L_i^r couplings at a NNLO precision. In this paper we present results for such a fit. Some studies using the extra observables but without performing a full new fit were reported in [10, 11, 12]. Notice that in a preliminary phase we converted all the FORTRAN programs used to evaluate the amplitudes up to NNLO into C++ code. Our fits are all performed using such programs.

The paper is organized as follows. In Section 2 we sketch out the ChPT formalism and its main underlying ideas. In Section 3 we review the phenomenological input we used in our results. We also show which are the L_i^r that give the largest contributions for each observable we included. Notice that now much more input is present compared to the past fits [8, 9]. In Section 4 we present the main model we used to estimate the C_i^r, i.e. the coupling constants appearing in the NNLO Lagrangian. Such an estimate is usually called the resonance estimate. In Section 5 we summarize the status of the main existing NNLO fit so far: fit 10 of [9]. In Section 6 we show our main findings using the C_i^r estimates of Section 4. We quote different fits so to show how each observable we include affects our findings. The best fit we get we call fit All and should be considered the main output of

this work. This fit exhibits several differences with fit 10. One especially striking feature is that it does not respect any longer the large N_c relation $2L_1^r \approx L_2^r$. We also show for fit All the convergence of the expansions for masses and decay constants, which is much improved compared to the one of fit 10. In Section 6.1 we perform a fit of the L_i^r using as input different experimental results for the $K_{\ell 4}$ amplitude. We show that with this input the large N_c relation $2L_1^r \approx L_2^r$ is better satisfied, although the resulting fit is not as good as fit All in convergence for the masses. In Section 6.2 we try to justify and test our estimate of the C_i^r. In Section 6.3 we compare further the fits obtained using their predictions for the two-flavour LECs $\bar{\ell}_i$. Fit All again results as the most convincing one. In Section 6.4 we show results for fits based on a different estimate of the C_i^r couplings that can be found in [13], this is essentially a chiral quark model estimate (CQM). The fits are not as good as fit All, nor for the χ^2 nor for the convergence of the expansions. Also in this case the large N_c relation is not satisfied. In Section 6.5 we provide a short comparison with the recent determination of L_5^r of [14].

In Section 7 we show results for an another treatment of the C_i^r. We let the C_i^r couplings to take random values, although they are forced to keep the size $1/(16\pi^2)^2$. These fits have been done requiring extra constraints of convergence for mass and decay constant expansions, as explained in Section 7.1. In this way it is easier to select only credible fits. The results of such a study are finally shown in Section 7.2. We found very many good fits that correctly predict all the observables used as input and with low χ^2. These fits are unfortunately different looking from each other. Therefore we can only show which are the ranges where we found the L_i^r to vary. For some of the NLO constants such ranges are very wide. This method shows however that it is possible to fit the NNLO expressions to the observables with C_i^r of the expected size and it also allows to study well the strong correlations between the couplings. Finally in the appendix we present a table where we quote our estimates for the NNLO couplings.

2 Chiral Perturbation Theory

We devote this section to a brief description of the formalism of three-flavour ChPT [1, 2, 3]. Introductory references are [15, 16]. The notation in the following is the same as in [4]. ChPT relies on the assumption that the flavour symmetry of QCD is spontaneously broken to the diagonal subgroup, $SU(3)_L \times SU(3)_R \to SU(3)_V$. According to the Goldstone theorem, 8 pseudo Goldstone bosons then arise. These are identified with the low lying pseudoscalar mesons and are organized in a unitary 3×3 matrix

$$u = \exp\left(\frac{i}{\sqrt{2}F}\phi\right) , \tag{1}$$

where ϕ is a hermitian 3×3 matrix:

$$\phi = \begin{pmatrix} \frac{1}{\sqrt{2}}\pi^0 + \frac{1}{\sqrt{6}}\eta & \pi^+ & K^+ \\ \pi^- & -\frac{1}{\sqrt{2}}\pi^0 + \frac{1}{\sqrt{6}}\eta & K^0 \\ K^- & \bar{K}^0 & -\frac{2}{\sqrt{6}}\eta \end{pmatrix} . \tag{2}$$

The Lagrangian describing the low-momentum strong interactions of the light mesons must be invariant under $SU(3)_L \times SU(3)_R$ local transformations. The most general lowest order Lagrangian is

$$\mathcal{L}_2 = \frac{F_0^2}{4} \left(\langle u_\mu u^\mu \rangle + \langle \chi_+ \rangle \right), \tag{3}$$

with

$$\begin{aligned} u_\mu &= i\{u^\dagger(\partial_\mu - ir_\mu)u - u(\partial_\mu - il_\mu)u^\dagger\}, \\ \chi_\pm &= u^\dagger \chi u^\dagger \pm u \chi^\dagger u, \\ \chi &= 2B_0(s + ip). \end{aligned}$$

The fields s, p, $l_\mu = v_\mu - a_\mu$ and $r_\mu = v_\mu + a_\mu$ are the standard external scalar, pseudoscalar, left- and right-handed vector fields introduced by Gasser and Leutwyler [2, 3]. The constants F_0 and B_0 are instead the leading-order (LO) LECs. The notation $\langle X \rangle$ stands for trace over up, down and strange quark flavour.

Starting from this Lagrangian we can then build up an effective field theory by including loop diagrams and higher order Lagrangians, where operators of higher dimensions are included. Their coupling constants are then counter-terms, i.e. their infinities absorb the UV divergences coming from the loop diagrams. In this way one obtains a theory renormalized order by order. Unfortunately going to higher orders the number of operators allowed by the symmetries increase and therefore also the number of unknown coupling constants. At NLO there are 10 LECs, called L_i^r, while at NNLO there are as many as 94, called C_i^r. We will always quote the renormalized versions where the C_i^r are made dimensionless by using the physical value of F_π. The renormalization scale is chosen to be $\mu = 770$ MeV. While there is in principle enough phenomenological information to fit the first ones, we still need to rely on theoretical models or on some other method for the latter ones, as those described in Sections 4, 6.4 and 7.

3 Fitting procedure and input observables

In this section we first show how we perform the fits and then we review shortly the observables we use as input and their values.

3.1 χ^2

The fit is performed using MINUIT in its C++ version [17, 18]. MINUIT is a routine to find the minimum value of a multi-parameter function. The procedure to perform the fits is very similar to the one explained in [9]. The function to be minimized is the χ^2 of the fit. It is obtained summing up the partial contributions $\chi^2_{i(\text{part})}$ for each input observables

$$\chi^2_{i(\text{part})} = \left(\frac{x_{i(\text{meas})} - x_{i(\text{calc})}}{\Delta x_i} \right)^2$$

$$\chi^2 \;=\; \sum_i \chi^2_{i(\mathrm{part})} \tag{4}$$

where $x_{i(\mathrm{meas})}$ are the physical values for each input observables and Δx_i their associated errors. $x_{i(\mathrm{calc})}$ are the results as calculated by ChPT up to NNLO. The rest of this section is devoted to list the values and the uncertainties used for each x_i.

3.2 Masses and decay constants

The masses and decay constants of the light pseudoscalar mesons have been calculated at NNLO in [19]. We use them as physical parameters, namely as input to calculate the several observables, similarly to what was done in [9]. Their values are given in [20] and are

$$\begin{aligned} m_{\pi^+} &= 139.57018 \text{ MeV}, \quad m_{\pi^0} = 134.9766 \text{ MeV}, \quad m_\eta = 547.853 \text{ MeV}, \\ m_{K^+} &= 493.677 \text{ MeV}, \quad m_{K^0} = 497.614 \text{ MeV}, \qquad (5) \\ F_\pi &= 0.0922 \pm 0.0002 \text{ GeV}\,. \qquad (6) \end{aligned}$$

The measurements in (5) and (6) differ slightly from the ones used in the latest full fit [9].

$$\begin{aligned} m_{\pi^+} &= 139.56995 \text{ MeV}, \quad m_{\pi^0} = 134.9764 \text{ MeV}, \quad m_\eta = 547.30 \text{ MeV}, \\ m_{K^+} &= 493.677 \text{ MeV}, \quad m_{K^0} = 497.672 \text{ MeV}, \qquad (7) \\ F_\pi &= 0.0924 \text{ GeV}\,. \qquad (8) \end{aligned}$$

Notice that preliminary results of our work have been reported in the proceedings [21, 22] and several unpublished talks. Those results were based on the masses of [23], that differ slightly from both (5), (6) and (7), (8).

All the new fits shown in this paper have been produced using the values in (5) and (6). However we have not observed any substantial modification of the outputs when using the old masses (7) and pion decay constant (8). As discussed below other changes in experimental input are behind the changes of central values.

The masses depend at LO on $B_0\hat{m}$ (with $\hat{m} = (m_u + m_d)/2$) and on $B_0 m_s$. L_4^r, L_6^r, L_5^r and L_8^r appear in the expression at NLO. In m_η^2 there is also a NLO contribution from L_7^r. The decay constant F_π depends instead on F_0, as an overall factor, and on L_4^r and L_5^r.

3.3 F_K/F_π

As input observable for our fits we will use the ratio F_K/F_π to eliminate the dependence on the unknown constant F_0, since it contributes as an overall factor for F_K as well. In the end the value of F_π then determines the value for F_0.

The ratio takes the value [20]

$$\frac{F_K}{F_\pi} = 1.197 \pm 0.007, \tag{9}$$

that is also in full agreement with several lattice estimates as reported in [24]. Using F_K/F_π at NLO we are sensitive to L_5^r. To perform the fit we expand the ratio as

$$\frac{F_K}{F_\pi} = 1 + \underbrace{\left.\frac{F_K}{F_0}\right|_{p^4} - \left.\frac{F_\pi}{F_0}\right|_{p^4}}_{\text{NLO}} + \underbrace{\left.\frac{F_K}{F_0}\right|_{p^6} - \left.\frac{F_\pi}{F_0}\right|_{p^6} - \left.\frac{F_K}{F_0}\right|_{p^4}\left.\frac{F_\pi}{F_0}\right|_{p^4} + \left.\frac{F_\pi}{F_0}\right|^2_{p^4}}_{\text{NNLO}}, \tag{10}$$

so that we can keep track of the exact contributions from the different orders. However we also check that the same quantity estimated as

$$\frac{F_K}{F_\pi} = \frac{F_0 + F_K|_{p^4} + F_K|_{p^6}}{F_0 + F_\pi|_{p^4} + F_\pi|_{p^6}} \tag{11}$$

gives approximately the same value[1].

Notice the experimental result for the ratio F_K/F_π (9) differs substantially from the one used in [9]. Ref. [9] used $F_K/F_\pi = 1.22 \pm 0.01$. The change in F_K/F_π is one of the major sources of difference with [9] as will be shown later in Section 6.

3.4 The quark-mass ratio $m_s/\hat{m}$

For the masses we have a similar problem, they depend on the quark masses and on B_0. We thus use as was done in [8, 9] the ratio of the strange quark mass over the isospin doublet quark mass $\hat{m}$ as input observable. The two following relations involving the light pseudoscalar meson masses hold at LO in ChPT

$$\left.\frac{m_s}{\hat{m}}\right|_1 = \frac{2m_{0K}^2 - m_{0\pi}^2}{m_{0\pi}^2} \qquad \left.\frac{m_s}{\hat{m}}\right|_2 = \frac{3m_{0\eta}^2 - m_{0\pi}^2}{2m_{0\pi}^2} \tag{12}$$

where with m_0 we indicate the meson masses at LO. They are calculated subtracting from the physical values the NLO and NNLO expressions. We include both relations in (12) in the fits. For the pion mass we use the neutral pion mass m_{π^0}. In the kaon case we need to correct the physical value for the mass since its electromagnetic contribution is sizeable. We take the average between m_{K^+} and m_{K^0} and then we subtract the electromagnetic contribution as stated by the Dashen's theorem and an estimate of its violation:

$$m_{K\text{av}}^2 = \frac{1}{2}(m_{K^+}^2 + m_{K^0}^2 - 1.8(m_{\pi^+}^2 - m_{\pi^0}^2)) = (494.50 \text{ MeV})^2. \tag{13}$$

The factor 1.8 in (13) is due to the corrections to Dashen's theorem where we use the value of [25].

The value of the quark mass ratio has been calculated by several lattice collaborations. The authors of [9] used as standard input $m_s/\hat{m} = 24$ with a 10% uncertainty, but they also

[1]We thank Veronique Bernard and Emilie Passemar for pointing out that these were significantly different for some of our preliminary fits.

checked that $m_s/\hat{m} = 26$ was compatible. Here instead we use $m_s/\hat{m} = 27.8$ as obtained by the Flavianet Lattice Averaging Group in [24], and we again adopt a 10% uncertainty for the error to be used in the fits when comparing with the theoretical values (12).

In the end the calculated NLO and NNLO masses are used to determine the lowest order mass or alternatively $B_0\hat{m}$.

3.5 $K_{\ell 4}$ formfactors

The decay $K^+(p) \to \pi^+(p_1)\pi^-(p_2)e^+(p_\ell)\nu(p_\nu)$ is given by the amplitude [7]

$$T = \frac{G_F}{\sqrt{2}} V_{us}^\star \bar{u}(p_\nu)\gamma_\mu(1-\gamma_5)v(p_\ell)(V^\mu - A^\mu). \tag{14}$$

In (14) V^μ and A^μ can be parametrized in terms of four formfactors: F, G, H and R. However the R-formfactor is negligible in decays with an electron in the final state. Using partial wave expansion and neglecting d wave terms one obtains for the F, G and the H formfactors [26]:

$$\begin{aligned} F(s_\pi, s_\ell, \cos\theta) &= f_s(s_\pi, s_\ell)e^{i\delta_s} + f_p e^{i\delta_p}\cos\theta + \dots, \\ G(s_\pi, s_\ell, \cos\theta) &= g_p(s_\pi, s_\ell)e^{i\delta_p} + \dots, \\ H(s_\pi, s_\ell, \cos\theta) &= h_p(s_\pi, s_\ell)e^{i\delta_p} + \dots, \end{aligned} \tag{15}$$

where we also assumed that the p phase is the same for the three formfactors. In (15) $s_\pi(s_\ell)$ is the invariant mass of dipion (dilepton) system, θ is the angle of the pion in their rest frame w.r.t. the kaon momentum. The F and G formfactors were calculated at NNLO in [8]. The quantities are especially sensitive to L_1^r, L_2^r and L_3^r. Also the H formfactor is known at order p^6 [27] but we do not use it as input observable since it depends on a different set of LECs, those from the anomalous intrinsic parity sector.

The measured observables are obtained by further parametrizing $f_s(s_\pi, s_\ell)$ and $g_p(s_\pi, s_\ell)$ as

$$\begin{aligned} f_s(s_\pi, s_\ell) &= f_s + f_s' q^2 + f_s'' q^4 + f_e' s_\ell/4m_\pi^2, \\ g_p(s_\pi, s_\ell) &= g_p + g_p' q^2, \end{aligned} \tag{16}$$

where $q^2 = s_\pi/(4m_\pi^2) - 1$. (16) can be used to fit the measured data points. In [9] the preliminary linear fit from the E865 measurement [28] was used as input. It has the values

$$f_s = 5.77 \pm 0.097, \quad f_s' = 0.47 \pm 0.15, \quad g_p = 4.684 \pm 0.092, \quad g_p' = 0.54 \pm 0.20. \tag{17}$$

Now more precise results from the NA48/2 experiment are available [29] and their second order fit of the formfactors read

$$\frac{f_s'}{f_s} = 0.152 \pm 0.009, \quad \frac{f_s''}{f_s} = -0.073 \pm 0.009, \quad \frac{g_p}{f_s} = 0.868 \pm 0.01, \quad \frac{g_p'}{f_s} = 0.089 \pm 0.02, \tag{18}$$

Notice that in [29] no measure of f_s is reported, therefore we always use the $f_s = 5.75 \pm 0.097$ from the E865 collaboration [30] in our fits. Multiplying by f_s and combining the errors in quadrature we obtain as measures

$$\begin{aligned} f_s &= 5.750 \pm 0.097, \quad f_s' = 0.874 \pm 0.054, \quad f_s'' = -0.420 \pm 0.052, \\ g_p &= 4.99 \pm 0.12, \quad g_p' = 0.512 \pm 0.121\,. \end{aligned} \tag{19}$$

In [29] there is also a linear fit which gives $\frac{f_s'}{f_s} = 0.073 \pm 0.004$ and thus $f_s' = 0.420 \pm 0.024$. Deciding which of the two fits for the F_s formfactor should be used is a relevant issue. The problem is how much we can rely on the curvature of the formfactor F_s. As a matter of fact it is difficult for NNLO ChPT to reproduce the large negative curvature f_s'', as was also noted in [9, 6]. A dispersive analysis approach combined to two loops ChPT, similar to the one done for $\pi\pi$ scattering [31], might clarify the situation. An indication of this is given by Figure 7 of [9]. It is visible there that the dispersive result for $K_{\ell 4}$ decay [7] has a larger curvature than the two-loop result [9].

Let us conclude with a cautionary remark about the $K_{\ell 4}$ data. In [32] it was made clear that isospin breaking effects at threshold give important corrections. These have not been taken into account in the NA48/2 analysis [29], thus they might affect significantly their findings.

3.6 $\pi\pi$ scattering

The $\pi\pi$ scattering amplitude can be written as a function $A(s,t,u)$ which is symmetric in t, u:

$$A(\pi^a\pi^b \to \pi^c\pi^d) = \delta^{a,b}\delta^{c,d}A(s,t,u) + \delta^{a,c}\delta^{b,d}A(t,u,s) + \delta^{a,d}\delta^{b,c}A(u,t,s)\,, \tag{20}$$

where s,t,u are the usual Mandelstam variables. The three flavour ChPT calculation of $A(s,t,u)$ was done in [11]. The isospin amplitudes $T^I(s,t)$ $(I = 0,1,2)$ are

$$\begin{aligned} T^0(s,t) &= 3A(s,t,u) + A(t,u,s) + A(u,s,t)\,, \\ T^1(s,t) &= A(s,t,u) - A(u,s,t)\,, \\ T^2(s,t) &= A(t,u,s) + A(u,s,t)\,, \end{aligned} \tag{21}$$

and are expanded in partial waves

$$T^I(s,t) = 32\pi \sum_{\ell=0}^{+\infty} (2\ell+1) P_\ell(\cos\theta) t_\ell^I(s), \tag{22}$$

where t and u have been written as $t = -\frac{1}{2}(s-4m_\pi^2)(1-\cos\theta)$, $u = -\frac{1}{2}(s-4m_\pi^2)(1+\cos\theta)$. In (22) we indicate with $P_\ell(\cos\theta)$ the Legendre polynomials. Near threshold the t_ℓ^I are further expanded in terms of the threshold parameters

$$t_\ell^I(s) = q^{2\ell}(a_\ell^I + b_\ell^I q^2 + \mathcal{O}(q^4)), \qquad q^2 = \frac{1}{4}(s - 4m_\pi^2), \tag{23}$$

a_0^0	0.220 ± 0.010	m_π^0
b_0^0	0.276 ± 0.012	m_π^{-2}
a_0^2	-0.444 ± 0.020	$10^{-1} m_\pi^0$
b_0^2	-0.803 ± 0.024	$10^{-1} m_\pi^{-2}$
a_1^1	0.379 ± 0.010	$10^{-1} m_\pi^{-2}$
b_1^1	0.567 ± 0.026	$10^{-2} m_\pi^{-4}$

Table 1: The values of the scattering lengths and slopes as found in [31] and our fitting uncertainties. In the third column the normalization factors are given. We quote here only those scattering parameters added as input in our fits.

where $a_\ell^I, b_\ell^I \ldots$ are the scattering lengths, slopes,.... These thresholds parameters constitute our observables. Currently a very precise determination of these parameters exists. It is based on a dispersive analysis approach and on two-flavour ChPT and can be found in [31]. In Table 1 we quote the values of the threshold parameters we use in our fits and their corresponding uncertainties, which we took to be double the ones in [31]. For most fits we used only a_0^0 and a_0^2 but we have checked that the others listed in Table 1 are also well within the uncertainties quoted. Notice also that the NA48/2 experiment in [29] obtained compatible values for a_0^0 and a_0^2 from the measurement of the $\delta = \delta_p - \delta_s$ phase shift in $K_{\ell 4}$ decays.

3.7 πK scattering

The πK scattering process has amplitudes $T^I(s,t,u)$ in the isospin channels $I = 1/2, 3/2$. They have been calculated at NNLO in ChPT in [12]. As for $\pi\pi$ scattering, it is possible to define scattering lengths and slopes a_ℓ^I, b_ℓ^I. So we introduce the partial wave expansion of the isospin amplitudes

$$T^I(s,t,u) = 16\pi \sum_{\ell=0}^{+\infty} (2\ell+1) P_\ell(\cos\theta) t_\ell^I(s), \tag{24}$$

where $P_\ell(\cos\theta)$ are the Legendre polynomials. Then we expand the $t_\ell^I(s)$ near threshold

$$t_\ell^I(s) = \frac{1}{2}\sqrt{s} q_{\pi K}^{2\ell} \left(a_\ell^I + b_\ell^I q_{\pi K}^2 + \mathcal{O}(q_{\pi K}^4) \right), \tag{25}$$

where

$$q_{\pi K}^2 = \frac{s}{4}\left(1 - \frac{(m_K + m_\pi)^2}{s}\right)\left(1 - \frac{(m_K - m_\pi)^2}{s}\right), \tag{26}$$

$a_0^{1/2}$	0.224 ± 0.044	m_π^{-1}
$b_0^{1/2}$	0.85 ± 0.08	$10^{-1} m_\pi^{-3}$
$a_0^{3/2}$	-0.448 ± 0.154	$10^{-1} m_\pi^{-1}$
$b_0^{3/2}$	-0.37 ± 0.06	$10^{-1} m_\pi^{-3}$
$a_1^{1/2}$	0.19 ± 0.02	$10^{-1} m_\pi^{-3}$
$b_1^{1/2}$	0.18 ± 0.04	$10^{-2} m_\pi^{-5}$
$a_1^{3/2}$	0.65 ± 0.88	$10^{-3} m_\pi^{-3}$
$b_1^{3/2}$	-0.92 ± 0.34	$10^{-3} m_\pi^{-5}$

Table 2: The values of the scattering lengths and slopes as found in [33]. The uncertainties quoted here are those used in our fits and are double the ones of [33]. In the third column the normalization factors are given. We quote only those scattering parameters added as input in our fits.

is the magnitude of the three-momentum in the center of mass system. The Mandelstam variables are given in terms of the scattering angle θ by

$$t = -2q_{\pi K}^2(1 - \cos\theta), \quad u = -s - t + 2m_K^2 + 2m_\pi^2 \,. \tag{27}$$

(25) defines the πK scattering parameters a_ℓ^I and b_ℓ^I that are our input observables. These have been computed from Roy and Steiner type equations in [33]. The results for the s and p waves scattering parameters we use are reported in Table 2. For most numerical results we used only $a_0^{1/2}$ and $a_0^{3/2}$ but we have checked that all the others agree within uncertainties.

3.8 Scalar formfactor

The scalar formfactor for the pion is defined as

$$F_S^\pi(t) = \langle \pi^0(p) | \bar{u}u + \bar{d}d | \pi^0(q) \rangle, \tag{28}$$

where $t = p - q$. Near $t = 0$ it is expanded via

$$F_S^\pi(t) = F_S^\pi(0) \left(1 + \frac{1}{6} \langle r^2 \rangle_S^\pi t + c_S^\pi t^2 + \dots \right) . \tag{29}$$

The observables $\langle r^2 \rangle_S^\pi$ and c_S^π are used as input in our fits. The NNLO ChPT calculation for these quantities was performed in [10]. The scalar formfactor cannot be measured experimentally. Measuring the $\pi\pi$ phase shifts and using a dispersive representation it is possible to infer its energy behaviour and therefore the values of $\langle r^2 \rangle_S^\pi$ and c_S^π [34, 35, 36]

$$\langle r^2 \rangle_S^\pi = 0.61 \pm 0.04 \text{ fm}^2, \qquad c_S^\pi = 11 \pm 2 \text{ GeV}^{-4}. \tag{30}$$

Notice that the result for $\langle r^2\rangle_S^\pi$ is also compatible with the lattice result of [37].

This is all the information we can extract from the scalar formfactors. Currently, there are basically no results available for $F_s^\pi(0)$ and for the energy behaviour of the kaon scalar formfactors or of the strange contribution to the pion formfactor.

3.9 L_9^r and L_{10}^r

We do not attempt to fit the remaining NLO LECs, L_9^r and L_{10}^r. Those LECs we fit are independent of L_9^r and L_{10}^r, or alternatively, none of the observables[2] we discuss depend on them. One needs to include additional information to constrain their values.

L_9^r appears alone at NLO in the electromagnetic radius of the pion vector formfactor. The NNLO contribution dependent on the other L_i^r is rather small [38]. It was therefore possible to fit that constant almost independently from the other couplings [38]. Furthermore it never appears at NLO in any of the observables used here as input thus it does not affect much our fits. We always set $L_9^r = (0.593 \pm 0.43) \times 10^{-2}$ for $\mu = 0.77$ GeV.

L_{10}^r can be estimated using τ decays data on the $V-A$ spectral function [39]. Its value was found to be $L_{10}^r = (-4.06 \pm 0.39) \times 10^{-3}$ at $\mu = 0.77$ GeV. However this constant never appears in the observables under study not even at NNLO. Therefore it does not have any influence on our fits. For this reason we always set such constant to zero in our fits.

4 Resonance estimates for the C_i^r

The many unknown coupling constants that appear in the p^6 Lagrangian, the C_i^r, represent the major problem for performing the fit with a $\mathcal{O}(p^6)$ precision. A lot of effort went into trying to estimate them using different models and treatments. The one we present here, also used in [8], is the resonance saturation model [40, 41]. It is based on the idea that the LECs encode the information from physics above $\Lambda_{\rm ChPT} \approx 1$ GeV, and that they are dominated by the physics just above this scale, i.e. the physics of low-lying resonances. Therefore we need a Lagrangian that describes these new particles and their interactions with the pseudoscalar mesons of the octet. We include only vector, scalar and the η' fields. We use the same estimate described in [8], thus we refer the reader to that paper for further details, including the Lagrangians used at the resonance level.

The model is used then to estimate the p^6 contributions depending on the C_i^r. In [8], the heavier mesons were integrated out producing p^6 Lagrangians for the pseudo-Goldstone boson. The heavy resonance fields for the vector mesons produce

$$\begin{aligned}\mathcal{L}_V &= -\frac{if_\chi g_V}{\sqrt{2}M_V^2}\langle\nabla_\lambda([u^\lambda,u^\nu])[u^\nu,\chi_-]\rangle + \frac{g_V\alpha_V}{\sqrt{2}M_V^2}\langle[u_\lambda,f_-^{\nu\lambda}](\nabla^\mu[u_\mu,u_\nu])\rangle \\ &\quad -\frac{ig_Vf_V}{2M_V^2}\langle(\nabla_\lambda f_+^{\lambda\nu})(\nabla^\mu[u_\mu,u_\nu])\rangle - \frac{i\alpha_Vf_\chi}{M_V^2}\langle[u_\nu,\chi_-][u_\lambda,f_-^{\nu\lambda}]\rangle\end{aligned}$$

[2] with the exception of $K_{\ell 4}$ where a very small dependence is present for $s_\ell \neq 0$.

$$-\frac{f_\chi f_V}{\sqrt{2}M_V^2}\langle(\nabla_\lambda f_+^{\lambda\mu})[u_\mu,\chi_-]\rangle\ , \tag{31}$$

and the scalar mesons

$$\mathcal{L}_S \ = \ \frac{c_d^2}{2M_S^4}\langle\nabla_\nu(u_\mu u^\mu)\nabla^\nu(u_\lambda u^\lambda)\rangle + \frac{c_m^2}{2M_S^4}\langle(\nabla_\nu\chi_+)(\nabla^\nu\chi_+)\rangle + \frac{c_d c_m}{M_S^4}\langle\nabla_\nu(u_\mu u^\mu)(\nabla^\nu\chi_+)\rangle\,. \tag{32}$$

While for the η' they obtained

$$\mathcal{L}_{\eta'} = -\frac{\tilde{d}_m^2}{2M_{\eta'}^4}\partial_\mu\langle\chi_-\rangle\partial^\mu\langle\chi_-\rangle \tag{33}$$

In (31) and (32) $f_\pm^{\mu\nu}$ are defined as

$$f_\pm^{\mu\nu} = u(v^{\mu\nu} - a^{\mu\nu})u^\dagger \pm u^\dagger(v^{\mu\nu} + a^{\mu\nu})u\,.$$

In [8] the above Lagrangians were not rewritten in the standard form of the Lagrangian at p^6. That work has since been done using more general resonance lagrangians in [42, 43]. We have checked that the results using the Lagrangians (31,32) directly agrees with the same inputs using the C_i^r directly in terms of resonance parameters as derived in [42, 43]. The η' contribution was rewritten in the C_i^r in [44].

The values we choose for the different couplings are the same as in [8]

$$\begin{aligned} &f_V = 0.20, \quad f_\chi = -0.025, \quad g_V = 0.09, \\ &\alpha_V = -0.014, \quad c_m = 42 \text{ MeV}, \quad c_d = 32 \text{ MeV}, \\ &\tilde{d}_m = 20 \text{ MeV}. \end{aligned} \tag{34}$$

and the masses are the experimental ones [20].

$$m_V = m_\rho = 0.77 \text{ GeV}, \qquad m_S = 0.98 \text{ GeV}, \qquad m_{\eta'} = 0.958 \text{ GeV}, \tag{35}$$

In Table 18 in the appendix we quote the C_i^r as estimated through the resonance model. We did not include more sophisticated resonance models because this would have again increased strongly the number of free parameters to be fitted. As discussed below we also have indications that terms suppressed by $1/N_c$, N_c the number of colours, might be important. These cannot at present be estimated using this type of approach.

5 Existing fits

In this section we describe a bit more in detail the earlier fits. The main full fit done is fit 10 in [9][3]. Earlier determination of the L_i^r did not fully include NNLO effects and we thus do not discuss them here. The values for the L_i^r obtained in fit 10 are reproduced in Table 3 in the column labelled fit 10. This is a full NNLO fit of the L_i^r and it was done including the quantities and the L_i^r whose value they influence most:

[3] The E865 data were still preliminary then, the main fit in [9] was with older $K_{\ell 4}$ data.

	fit 10	fit 10 iso
$10^3 L_1^r$	0.43	0.39 ± 0.12
$10^3 L_2^r$	0.73	0.73 ± 0.12
$10^3 L_3^r$	-2.35	-2.34 ± 0.37
$10^3 L_4^r$	$\equiv 0$	$\equiv 0$
$10^3 L_5^r$	0.97	0.97 ± 0.11
$10^3 L_6^r$	$\equiv 0$	$\equiv 0$
$10^3 L_7^r$	-0.31	-0.30 ± 0.15
$10^3 L_8^r$	0.60	0.60 ± 0.20
χ^2 (dof)	- -	0.26 (1)

Table 3: The results for fit10 of [8] and for a similar fit done without including isospin breaking corrections for the masses (fit10 iso) and also using the masses in (5) and decay constant F_π as in (6). The uncertainties are those calculated by MINUIT. The two fits reported are in agreement within uncertainties.

	p^2	p^4	p^6
m_π^2	0.753	0.006	0.241
m_K^2	0.702	0.007	0.291
m_η^2	0.747	-0.047	0.300
F_π/F_0	1	0.136	-0.075
F_K/F_0	1	0.307	-0.003
F_K/F_π	1	0.171	0.049

Table 4: The convergence of the expansion for the meson masses and the decay constants for fit 10 iso. A similar behaviour holds for fit10. The masses quoted are normalized to the physical masses, while the decay constants to F_0 ($F_0 = 0.0869$ GeV).

1. masses and pion decay constant with the old values as in (7) and (8)

2. the $K_{\ell 4}$ formfactor parameters: f_s, f_s', g_s, g_s'. They constrained mostly L_1^r, L_2^r, L_3^r.

3. $F_K/F_\pi = 1.22 \pm 0.01$, sensitive to L_5^r.

4. $m_s/\hat{m} = 24$ constrains L_7^r, L_8^r via the masses in (12).

5. $L_4^r \equiv L_6^r \equiv 0$ since they are $1/N_c$ suppressed couplings.

The C_i^r contributions were estimated using resonance saturation as described in Section 4. They also included there the axial-vector resonances, although their contribution was rather small. The scale of saturation was set to $\mu \equiv 0.77\,\mathrm{GeV}$, but $\mu = 0.5,\, 1\,\mathrm{GeV}$ were within errors. In fit 10 isospin breaking corrections in the masses and decay constants were also included, though the authors of [9] noticed that the neglect of isospin violation was a good approximation. Indeed the fits performed including or not these effects are in agreement within errors as can be seen from Table 3 comparing the columns fit 10 and fit 10 iso.

Fit 10 has been so far a quite successful fit. Not only because it already included many quantities at order p^6, but also because the resulting L_i^r nicely confirmed the estimates from resonance models. These are lead by the large N_c expansion which predicts e.g. $2L_1^r \approx L_2^r$ and $L_4^r \approx L_6^r \approx 0$. While the second relation was imposed, the first one was found to be well satisfied. This added credibility to the fit itself even though it relied on the resonance estimate for the tree-level p^6 contributions.

However the convergence of the perturbative expansion for this fit is not as expected. The different orders for the masses and decay constants are reported in Table 4 for fit 10 iso[4]. The $\mathcal{O}(p^4)$ order of the masses turns out to be tiny, far less than the expected 30%. On the other hand the NNLO contribution is definitely too large. The sources of this bad convergence are basically two. First the constraint $L_4^r \equiv L_6^r \equiv 0$ that clearly sends to zero many contributions coming from the NLO tree-level diagrams. Secondly most of the C_i^r appearing in the masses expressions are estimated to be zero as well. Therefore they cannot help in canceling large two-loop contributions. On the other hand the convergence for the decay constants is quite satisfying.

After fit 10 was performed many other observables have been calculated at $\mathcal{O}(p^6)$ in $SU(3)$ ChPT such as the $\pi\pi$ and πK scattering threshold parameters. Of course it is very important to compare the pure ChPT predictions obtained using fit 10 with the values of Tables 1 and 2. These comparisons have been done and can be found in Table 1 of [11] and in Table 4 of [12]. Fit 10 is mostly in agreement within errors, although there are small discrepancies in some of the threshold parameters. Some comparison with scalar formfactors was done in [10]. The last three papers used the same inputs as fit 10 and tried to vary L_4^r and L_6^r to see if some preferred regions could be found. Here we redo the fit from the beginning with all inputs.

[4]The numbers for fit 10 itself can be found in Table 2 of [10].

	fit 10 iso	NA48/2	F_K/F_π	All $\star$	All	$C_i^r \equiv 0$	All p^4
$10^3 L_1^r$	0.39 ± 0.12	0.88	0.87	0.89	0.88 ± 0.09	0.65	1.12
$10^3 L_2^r$	0.73 ± 0.12	0.79	0.80	0.63	0.61 ± 0.20	0.11	1.23
$10^3 L_3^r$	-2.34 ± 0.37	-3.11	-3.09	-3.06	-3.04 ± 0.43	-1.47	-3.98
$10^3 L_4^r$	$\equiv 0$	$\equiv 0$	$\equiv 0$	0.60	0.75 ± 0.75	0.80	1.50
$10^3 L_5^r$	0.97 ± 0.11	0.91	0.73	0.58	0.58 ± 0.13	0.68	1.21
$10^3 L_6^r$	$\equiv 0$	$\equiv 0$	$\equiv 0$	0.08	0.29 ± 0.85	0.29	1.17
$10^3 L_7^r$	-0.30 ± 0.15	-0.30	-0.26	-0.22	-0.11 ± 0.15	-0.14	-0.36
$10^3 L_8^r$	0.60 ± 0.20	0.59	0.49	0.40	0.18 ± 0.18	0.19	0.62
χ^2	0.26	0.01	0.01	1.20	1.28	1.67	2.60
dof	1	1	1	4	4	4	4

Table 5: Several global fits compared to fit10 iso. For all the fit $\mu = 0.77$ GeV. The errors quoted are the ones as calculated by MINUIT. The numbers in the row labelled dof are the degrees of freedom for the fit. See the description in the text for further details on how the fits have been performed. The column labelled All is our main new result.

6 New Fits

The aim of this section is to show how the new measurements and observables included in our global fits, change the results compared to fit 10. We have rewritten as mentioned above all programs into C++ and are using the isospin symmetric versions of the calculations. We therefore first redid the fit using the same inputs as fit 10. The outputs are given in Table 3 in the column labelled fit 10 iso. This also shows that the minor changes in masses and F_π as well the isospin breaking corrections do not affect the fit values appreciably. We will now add the effects of the changed experimental inputs and of the additional inputs to see how they change the fitted values of the L_i^r.

In Table 5 we present several fits. These have all been performed using the resonance estimate of the C_i^r of Section 4 and Table 18 in the appendix, setting the scale of saturation $\mu = 0.77$ GeV. Furthermore, we used the new values of the masses and decay constant of (5) and (6). We remind the reader that the use of these new parameter-values affects the output only within the uncertainties. Hereafter we summarize the steps in which we have included the new information.

NA48/2 The input observables and their values are the same as for fit 10 iso, but we use the new measurements in (19) for the $K_{\ell 4}$ decay from the NA48/2 collaboration [29]. The new measurements lead immediately to a striking feature: the large N_c relation $2L_1^r \approx L_2^r$ does not hold any longer. It even turns out that $L_2^r \lesssim L_1^r$. Notice that, as explained in Section 3.5, the slope f_s' comes from a second order fit of the f_s formfactor and therefore it differs from the one used in fit 10. In Section 6.1 we will present also results for the linear fit of the f_s formfactor.

F_K/F_π Same as fit NA48/2 but with the new value in (9) for F_K/F_π. L_5^r is mainly affected

and becomes smaller than in fit 10. As a consequence also the convergence of the decay constants expansion is worsened, e.g. $F_\pi/F_0|_{p^4} \approx 0.134$ while $F_\pi/F_0|_{p^6} \approx -0.126$.

All$\star$ In this fit we include a few more observables, i.e. the $\pi\pi$ scattering parameters a_0^0 and a_2^0, the πK scattering parameters $a_0^{\frac{1}{2}}$ and $a_0^{\frac{3}{2}}$ and the pion scalar radius $\langle r\rangle_S^2$. We also release the constraint $L_4^r = L_6^r = 0$ because now we have many more observables included. Unfortunately since none of the new observables involve information on the masses (and therefore on those two couplings), we still cannot achieve the precise values of L_4^r and L_6^r. They are highly correlated and MINUIT gives a very large uncertainty for those. Furthermore since now the $\mathcal{O}(p^4)$ contributions to the masses due to L_4^r and L_6^r are not zero, L_5^r and L_8^r diminish.

All This fit is very similar to fit All$\star$. Here we adopt the new value for the quark mass ratio $m_s/\hat{m} = 27.8$. However we find that using values for the quark mass ratio between 27 and 29 does not change the results considerably. The constants L_7^r, that appears in the η mass, and L_8^r are strongly affected by this change. This is also relatively true for L_4^r and L_6^r. We also tried to perform the same fit but setting $L_4^r \equiv L_6^r \equiv 0$. The resulting fit is very similar to fit NA48/2 but it has a huge χ^2 ($\chi^2 = 45$).

$C_i^r \equiv 0$ In the last column of the table we quote the fit obtained including the same input as for fit All, but setting all the $C_i^r \equiv 0$. This fit has been done to show how the different C_i^r can affect the L_i^r fit. Notice that the constants L_1^r, L_2^r and L_3^r change a lot, while the others stay in the same area as in fit All. This is not surprising: the last few constants are indeed primarly fitted from quantities where many contributing C_i^r are large-N_c suppressed and those which are not are set to zero also in the simple resonance estimate used.

All p^4 Same fit as All but all expressions are now at NLO. Use this fit for one-loop ChPT results. Note that this produces very high values for L_4^r and L_6^r. The underlying reason is that the lower value of F_K/F_π requires a smaller L_5^r than before and the pion scalar radius then requires at this order a larger L_4^r. This effect is also visible in fit All but is reduced when including the NNLO corrections.

Fit All is what we consider as the present best fit for NNLO ChPT calculations, it thus superseeds fit 10 of [9].

Let us discuss how the ChPT expansion is affected by the new values for the L_i^r. The various terms of the mass expansions read for fit All

$$\begin{array}{lll} m_\pi^2|_{p^2} = 1.035 & m_\pi^2|_{p^4} = -0.084 & m_\pi^2|_{p^6} = +0.049\,, \\ m_K^2|_{p^2} = 1.106 & m_K^2|_{p^4} = -0.181 & m_K^2|_{p^6} = +0.075\,, \\ m_\eta^2|_{p^2} = 1.186 & m_\eta^2|_{p^4} = -0.224 & m_\eta^2|_{p^6} = +0.038\,, \end{array} \tag{36}$$

	$K^0_{\ell 3}$	$K^+_{\ell 3}$
p^4	-0.02276	-0.02287
p^6 loops only	0.1141	0.01115
p^6-L_i^r fit 10 iso	0.00342	0.00330
p^6-L_i^r fit All	0.00232	0.00247

Table 6: The results for $f_+(0)$ in the two $K_{\ell 3}$ decays. This is an update of Table 3 in [45]

while those for the decay constants are

$$\begin{aligned} \left.\frac{F_\pi}{F_0}\right|_{p^4} &= 0.311 \quad \left.\frac{F_\pi}{F_0}\right|_{p^6} = 0.108 \\ \left.\frac{F_K}{F_0}\right|_{p^4} &= 0.441 \quad \left.\frac{F_K}{F_0}\right|_{p^6} = 0.216\,, \\ \left.\frac{F_K}{F_\pi}\right|_{p^4} &= 0.129 \quad \left.\frac{F_K}{F_\pi}\right|_{p^6} = 0.068\,. \end{aligned} \tag{37}$$

In (36) and (37) we used the same normalizations as in Table 4, although now $F_0 = 0.065$ GeV, this is due to the larger value of L_4^r which comes however with a large error. Notice that the convergence of the mass expansions in (36) is improved compared to the one of fit 10 in Table 4. However (36) looks strange: the LO masses are larger than the physical ones and there are significant cancellations between NLO and NNLO. Furthermore, even if the convergence is improved, it is still quite different from the one expected. E.g. the $m_\pi^2|_{p^4}$ contribution is much smaller than the expected 30% and it is of the same size as the p^6 order. The convergence for the decay constants is a bit worsened compared to the one of fit 10, due to the low value of L_5^r, but it is still acceptable. Notice also that when the ratio F_K/F_π is calculated with (11) the resulting value is 1.168, which is 3% smaller than the expected 1.197 . This can be due to higher order corrections that are included in the ratio of (11), but not in (10).

We performed more fits than those quoted in Table 5. We included more $\pi\pi$ scattering parameters and πK scattering parameters. We found that these fits are compatible with fit All of Table 5 within uncertainties. The same is true when we add the quantity c_s^π.

For completeness we quote the value for $f_+(0)$, the formfactor of $K_{\ell 3}$ decay at zero momentum transfer. This quantity was calculated at NNLO in [45]. We check how much the new L_i^r of fit All would affect its value. Notice that at zero momentum the dependence on L_9^r drops out. The other L_i^r appear only at NNLO. We discuss both the case of the charged kaon, the $K^+_{\ell 3}$ decay, and the neutral one $K^0_{\ell 3}$. The results we obtain using the masses of the particles involved in the decay are given in Table 6. These numbers can be seen as an update of those in Table 3 of [45]. The numbers for the pure loops are changed w.r.t. [45] mainly because of the change in F_π. Fit 10 iso is essentially the same as fit 10 used in [45] but has a small (1%) difference. The L_i^r-dependent contribution changes but since it stays small the total result is very similar to [45]. The total value for $f_+(0)$ for $K^+_{\ell 3}$

is instead

$$f_+(0)|_{\mathrm{C_i}=0(L_i^r=\mathrm{fit10})} = 0.9916, \qquad f_+(0)|_{\mathrm{C_i}=0(L_i^r=\mathrm{fitAll})} = 0.9908 \tag{38}$$

and for $f_+(0)$ for $K^0_{\ell 3}$ is instead

$$f_+(0)|_{\mathrm{C_i}=0(L_i^r=\mathrm{fit10})} = 0.9921, \qquad f_+(0)|_{\mathrm{C_i}=0(L_i^r=\mathrm{fitAll})} = 0.9910. \tag{39}$$

By comparing the two results in (38) and in (39) one realizes that the differences due to the L_i^r have a very small effect on $f_+(0)$.

The main uncertainty still remains the value of the contribution of the C_i. The estimate for the relevant constants used in this paper leads to $f_+(0)|_{C_i} \approx -0.045$ but the fitting inputs used here do not strongly constrain the relevant combination.

6.1 Linear fit for $K_{\ell 4}$ decays

One of the most striking features of the results presented in Table 5 is that as soon as the new results from the quadratic fit of the NA48/2 collaboration [29] are included, the constants L_1^r and L_2^r take unexpected values. Indeed, as was noted above, they do not respect any longer the large-N_c relation $2L_1^r \approx L_2^r$, but already in fit NA48/2 they are $L_1^r \approx L_2^r$ while when also the $\pi\pi$ and the πK scattering lengths are included (fit All) we even obtain $L_1^r > L_2^r$. On the other hand when we calculate the curvature f_s'' using the L_i^r as obtained in fit All we obtain $f_s'' = -0.124$ to be contrasted with the experimental value $f_s'' = -0.437$. Furthermore, whenever we include as input also f_s'' we again obtain fits compatible to the ones in Table 5, but with much larger χ^2 (e.g. $\chi^2 \sim 35$ for fit All) and the largest contribution comes exactly from f_s''. These results confirm what was already stated at the end of Section 3.5, i.e. the state-of-art ChPT does not reproduce such a large negative bend. Since f_s' and f_s'' are highly correlated, the linear and the quadratic fit of the F_s formfactor present rather different slopes.

For such reasons we perform fits using the slope of the linear fit $f_s'/f_s = 0.073$ [29] as well. The resulting fit, analogous to fit All, is reported in Table 7. By inspection one can see that the large N_c relation $2L_1^r = L_2^r$ still does not precisely hold, but at least $1.4L_1^r \approx L_2^r$. On the other hand L_4^r and L_6^r are again not suppressed, while L_7^r and L_8^r are unexpectedly small. Also all the constants have large uncertainties.

The convergence of the chiral expansions is worse than the one for fit All. The various terms of the mass expansions read

$$\begin{array}{lll} m_\pi^2|_{p^2} = 0.655 & m_\pi^2|_{p^4} = 0.370 & m_\pi^2|_{p^6} = -0.025\,, \\ m_K^2|_{p^2} = 0.699 & m_K^2|_{p^4} = 0.181 & m_K^2|_{p^6} = 0.120\,, \\ m_\eta^2|_{p^2} = 0.751 & m_\eta^2|_{p^4} = 0.151 & m_\eta^2|_{p^6} = 0.098\,, \end{array} \tag{40}$$

while those for the decay constants are

$$\left.\frac{F_\pi}{F_0}\right|_{p^4} = 0.355 \qquad \left.\frac{F_\pi}{F_0}\right|_{p^6} = 0.157$$

	All linear
$10^3 L_1^r$	0.58 ± 0.10
$10^3 L_2^r$	0.80 ± 0.12
$10^3 L_3^r$	-3.33 ± 1.42
$10^3 L_4^r$	0.93 ± 0.31
$10^3 L_5^r$	0.71 ± 0.24
$10^3 L_6^r$	0.86 ± 0.87
$10^3 L_7^r$	-0.04 ± 0.40
$10^3 L_8^r$	0.02 ± 0.79
χ^2(dof)	1.16(4)

Table 7: The analogous of fit All, but the linear fit of the $K_{\ell 4}$ formfactors have been used. The values of the L_i^r are at $\mu = 0.77$ GeV.

$$\left.\frac{F_K}{F_0}\right|_{p^4} = 0.498 \quad \left.\frac{F_K}{F_0}\right|_{p^6} = 0.262\,, \qquad (41)$$
$$\left.\frac{F_K}{F_\pi}\right|_{p^4} = 0.143 \quad \left.\frac{F_K}{F_\pi}\right|_{p^6} = 0.054\,.$$

In the light of these results it is rather difficult to draw a conclusion. The very different predictions for L_1^r and L_2^r obtained in fit All and this fit confirm that the picture of ChPT for $K_{\ell 4}$ decays is still incomplete. As mentioned earlier, we expect a dispersive analysis to produce a larger curvature.

6.2 Some small variations on fit All

In the resonance estimate described in Section 4 there is at least an assumption not entirely justified. We assume the scale at which the saturation happens to be 0.77 GeV, i.e. the mass of the lowest lying resonance. Nothing prevents us to choose a larger or smaller scale, although this is still expected to be in the same range of energy. To check whether this assumption is safe we try to fit from data the saturation scale parameter as well. The results are rather reassuring. Fit All of Table 5 is completely unaffected by this procedure. The fitted saturation scale is 0.77 ± 0.45 GeV.

The fit in Table 7 shows a little difference. The fitted saturation scale is now 0.71 ± 0.31 GeV. However the L_i^r do not change that much and the look of the fit is pretty much the same as before.

We also attempt to find better estimates of the C_i^r constants releasing the values of the couplings g_V, c_d and c_m. Again we try to fit them using both the input of fit All and of the fit in Table 7 (linear fit of NA48/2 instead of quadratic). In the first case we find in fact g_V and c_m close to the ones in (34). They read $g_V = 0.097 \pm 0.123$ and $c_m = 0.045 \pm 0.049$ GeV. For c_d we find instead a value larger than expected, i.e. $c_d = 0.093 \pm 0.100$ GeV. Anyway they are all affected by large uncertainties. The L_i^r fit is somewhat compatible with the one

	fit 10 iso	All	All linear	[31, 24]
$\bar{\ell}_1$	$-0.6(0.5)$	$-0.1(1.1)$	-1.9	-0.4 ± 0.6
$\bar{\ell}_2$	5.7(4.9)	5.3(4.6)	5.7	4.3 ± 0.1
$\bar{\ell}_3$	1.3(2.9)	4.2(4.9)	4.1	3.3 ± 0.7
$\bar{\ell}_4$	4.0(4.1)	4.8(4.8)	4.5	4.4 ± 0.4

Table 8: The values of the scale-independent $SU(2)$ LECs $\bar{\ell}_i$. In the first three columns we show the values as predicted by fit 10, fit All and fit All linear using the NNLO matching conditions of [46]. The numbers between parenthesis are the NLO results. In the last column we quote the known values from [31, 24]. Notice that the uncertainty over $\bar{\ell}_4$ is double the one quoted in [31] due to the still unclear situation for the lattice results [24].

of Table 5, fit All, within uncertainities because of the large ranges allowed for g_V, c_m, c_d. The fits are in a very broad minimum here with only one degree of freedom.

If we apply the same procedure but with the same $K_{\ell 4}$ input as for Table 7 (NA48/2 linear fit) we arrive to similar conclusions: the values of g_V and c_d are similar to the ones in (34), while c_d is larger. Again all the resonance couplings present large uncertainties. The L_i^r are here rather well compatible with those in Table 7.

We also try to multiply the C_i^r by an overall constant α and include it as a fitting parameter. It is encouraging to see that the result is $\alpha \approx 1.03$, namely the best fit is reached with basically the same values of the C_i^r from resonance estimate. Obviously the fit obtained is very similar to fit All. When we apply the same procedure to the fit in Table 7 the constant α takes the value 0.90. This affects the fit of Table 7, but still within uncertanties.

From this we conclude that fit All is stable against small changes in the resonance estimate of the C_i^r.

6.3 Adding input: $\bar{\ell}_i$ constants in two-flavour ChPT

The authors of [46, 47] study three flavour ChPT in the limit where the m_s is assumed to be much larger than $\hat{m}$ and the external momenta. In this case they can integrate out the strange quarks and $SU(3) \times SU(3)$ ChPT reduces to $SU(2) \times SU(2)$ ChPT. Matching the results from the two frameworks they calculate explicitely the dependence of the two-flavour LECs (the scale-independent $\bar{\ell}_i$ and the c_i^r) on the strange quark mass and on the three-flavour LECs. These relations have been worked out using two different methods at order p^6 in [46, 47].

There exist different evaluations of the $\bar{\ell}_i$. $\bar{\ell}_3$ has been estimated rather well using lattice results [24]. $\bar{\ell}_1$, $\bar{\ell}_2$, $\bar{\ell}_4$ and $\bar{\ell}_6$ have been obtained by matching two-flavour ChPT with dispersive results [31], but (contradictory) lattice results exist for those too [24]. We have increased the error on $\bar{\ell}_4$ because of this.

In Table 8 we summarize all the values of these constants and the results obtained by plugging the L_i^r and C_i^r of fit 10 iso, fit All and fit All linear in both the NNLO and

NLO relations of [46, 47]. By comparison of the first three columns with the last one of Table 8 it is easy to see that none of the fits correctly reproduces all the $\bar{\ell}_i$ values. A similar conclusion holds also for the fit in the next-to-last column of Table 5, where all the C_i^r are zero. The disagreement with the $\bar{\ell}_i$ in this case is actually even stronger. These fits encounter particular trouble in fitting $\bar{\ell}_2$.

We tried to fit the $\bar{\ell}_i$ whose values appear on the last column of Table 8 in addition to the inputs used for fit All. Not surprisingly it is not possible to accommodate all those inputs at the same time. The resulting χ^2 is approximately 22 and its largest contributions come exactly from the $\bar{\ell}_i$. Excluding from the fit $\bar{\ell}_2$ but including the others improves the situation. The resulting L_i^r values are very close to the ones of fit All, the most important deviation being $10^3 L_3^r = -3.18$. The χ^2 takes the value 3.15 with 7 degrees of freedom. Also in this case the value for $\bar{\ell}_2$ is still far from the expected one.

This is not surprising. In [46] it was found that the constant $\bar{\ell}_2$ depends on the couplings L_2^r, L_3^r and on the combination $2C_{13}^r - C_{11}^r$. The authors of [46] observed there that to find agreement with the determined value of $\bar{\ell}_2$ the combination of C_i^r must not be zero. Unfortunately those are two large-N_c suppressed couplings and therefore they are set to zero in our resonance estimate (see Table 18). We also try to fit those two C_i^r using also $\bar{\ell}_2$ as input observable, but this has been unsuccessful as well. In this way we manage to accommodate the value for $\bar{\ell}_2$, but then $\bar{\ell}_1$ is off, since it contains also a different combination of C_{11}^r, C_{13}^r and of C_6^r. This last coupling is also N_c-suppressed and thus estimated to be zero. In the end there is no way out: when we try to fit C_6^r too, there are other quantities taking very different values. The C_i^r are too correlated to be able to fit only a few of them.

As far as regards the fit in Table 7 the results for the $\bar{\ell}_i$ are even less clear. Its predictions are reported in the third column of Table 8. It is straightforward to see that now even the predicted $\bar{\ell}_1$ is off. Of course when we try to fit all the $\bar{\ell}_i$ the χ^2 is very large ($\chi^2 \approx 37.7$). Contrary to what happened for fit All, the situation does not improve that much when we exclude $\bar{\ell}_2$. For this fit seems to be very hard to reach the correct value for $\bar{\ell}_1$ too. The resulting χ^2 in this second case is 5.82 with $\bar{\ell}_1 = -1.4$.

Finally an extra cautionary remark. Requiring that the $SU(3)$ ChPT constants predict the values for the $SU(2)$ ones might not be a very safe assumption. What it assumes is that both $SU(2)$ and $SU(3)$ ChPT work well for the same quantities. For the $\pi\pi$ scattering quantities, which are very much determined by loop parts, relatively small differences can become amplified in the resulting values of the LECs.

6.4 A chiral quark model estimate for the C_i^r

We discussed above a simple resonance saturation estimate for the NNLO LECs C_i^r. There are other attempts at predicting these values as well from chiral quark models. As a representative of this we choose [13]. It also is a large N_c approximation but with a somewhat different pattern than our resonance saturation. Their method is based on a study of the relation between the chiral Lagrangian up to order p^6 and QCD, they find as expected that the LECs can be given in terms of some Green functions of QCD. In

	C_i^r[13]	$\alpha \times C_i^r$[13]
$10^3 L_1^r$	0.66 ± 0.11	0.66 ± 0.10
$10^3 L_2^r$	0.59 ± 0.13	0.24 ± 0.32
$10^3 L_3^r$	-2.74 ± 0.48	-1.80 ± 0.75
$10^3 L_4^r$	0.75 ± 0.16	0.77 ± 0.84
$10^3 L_5^r$	1.64 ± 0.83	0.83 ± 0.39
$10^3 L_6^r$	0.64 ± 0.41	0.32 ± 0.99
$10^3 L_7^r$	-0.25 ± 0.30	-0.15 ± 0.14
$10^3 L_8^r$	0.76 ± 0.75	0.27 ± 0.23
α	–	0.27 ± 0.47
χ^2 (dof)	3.71 (4)	1.35 (3)

Table 9: The results as obtained using the C_i^r estimates of [13]. Both the fits include the same observables as fit All of Table 5. In the second column the coefficient α multiplied by the C_i^r has been included as fitting parameter. The L_i^r are given at $\mu = 0.77$ GeV.

	p^2	p^4	p^6
m_π^2	0.988	-0.066	0.078
m_K^2	1.056	-0.177	0.121
m_η^2	1.131	-0.225	0.094
F_π/F_0	1	0.318	0.108
F_K/F_0	1	0.475	0.198
F_K/F_π	1	0.156	-0.050

Table 10: The results as obtained using the C_i^r estimates of [13] showing the convergence for the fit where α is left free. The normalizations are the same as explained in Table 4. Now $F_0 = 0.065$ GeV.

the evaluation of these Green functions, several assumptions and approximations are made such that it is not a full derivation but something like a chiral quark model. Their results are presented in Table IV of [13].

We also use their estimate to perform the fits. The results can be found in Table 9. There are results for two different fits. They have been obtained including all the observables as for fit All of Table 5. In the first column we use the C_i^r as quoted in Table IV of [13], whereas in the second column we multiply them by an overall constant α that is also fitted. This second fit was done because we observed that the values for the C_i^r of [13] are somewhat larger than the ones of the resonance estimates of Table 18. The fit confirms this observation and finds as best value for $\alpha = 0.27$, i.e. C_i^r considerably smaller than the ones in [13]. The value of the χ^2 for the two fits of Table 9 is somewhat worse than for fit All. Indeed it seems that it is now very difficult to fit the slope g_p' of the G formfactor for $K_{\ell 4}$ decay. From the second fit of Table 9 one can notice that when the C_i^r are allowed to

	C_i^r [13]	$\alpha \times C_i^r$ [13]
$10^3 L_1^r$	0.38 ± 0.10	0.35 ± 0.11
$10^3 L_2^r$	0.88 ± 0.12	0.43 ± 0.30
$10^3 L_3^r$	-3.20 ± 0.47	-2.04 ± 0.79
$10^3 L_4^r$	0.42 ± 0.17	0.91 ± 0.35
$10^3 L_5^r$	1.62 ± 0.77	1.03 ± 0.57
$10^3 L_6^r$	0.43 ± 0.21	0.87 ± 0.77
$10^3 L_7^r$	-0.32 ± 0.45	-0.11 ± 0.34
$10^3 L_8^r$	0.92 ± 1.07	0.17 ± 0.71
α	–	0.22 ± 0.47
χ^2 (dof)	4.13 (4)	1.20 (3)

Table 11: The results as obtained using the C_i^r estimates of [13]. Both the fits include the same observables as the fit in Table 7, i.e. as fit All but with the linear fit from NA48/2. In the second column the coefficient α multiplied by the C_i^r has been included as fitting parameter. The L_i^r are given at $\mu = 0.77$ GeV.

	p^2	p^4	p^6
m_π^2	0.624	0.384	-0.008
m_K^2	0.667	0.189	0.144
m_η^2	0.716	0.149	0.135
F_π/F_0	1	0.354	0.142
F_K/F_0	1	0.531	0.225
F_K/F_π	1	0.177	-0.020

Table 12: The convergence for the fit where α is left free is shown. The normalizations are the same as explained in Table 4. Now $F_0 = 0.062$ GeV. Fit as in rightmost column of Table 11.

take smaller values the L_2^r constant compensates for that. This allows the fit to reach a better value for the g_p'.

As can be seen in Table 10, even the convergence for the masses and decay constants is worse than the one for fit All reported in (36) and (37) respectively. Notice that we have not quoted the convergence for the fit obtained without multiplying the C_i^r by the coefficient α. In fact this is found to be even worse than the one of Table 9, the p^4 terms being constantly larger than, although comparable in size to, the p^6 ones.

In Table 11 and 12 we quote the results obtained with the C_i^r of [13], but fitting the slope of the linear fit for the F_s formfactor as in the fit of Table 7. Conclusions similar to the ones drawn for Table 9 hold here too.

	[14]	fit All	best reso	best rand
$10^3 L_5^r$	0.76 ± 0.09	0.58 ± 0.13	1.40 ± 0.009	1.40 ± 0.009
$10^5 C_{14}^r + C_{15}^r$	0.31 ± 0.07	0	-0.99	-1.06
$10^5 C_{15}^r + 2C_{17}^r$	1.10 ± 0.14	0	0.02	2.01

Table 13: The values of the couplings L_5^r, $C_{14}^r + C_{15}^r$ and $C_{15}^r + 2C_{17}^r$ as obtained from a fit to lattice data [14] (second column) and from our fits. Notice that the resonance model used for fit All estimates the combinations of C_i^r occurring here as zero. The columns best reso and best rand are taken from Tables 16 and 18 and are discussed in Section 7. All the values are at the scale $\mu = 0.77$ GeV.

6.5 Comparison with a recent L_5^r determination

The authors of [14] propose a simplification of the NNLO predictions of ChPT to perform fits to lattice data points. As an example they fit the lattice results [48] for F_K/F_π with their approximation to the two-loop ChPT prediction. Since too many couplings appear at NNLO they are forced to fit only a few of them and fix the others. They decide to fit L_5^r and the only two C_i^r-combinations contributing: $C_{14}^r + C_{15}^r$ and $C_{15}^r + 2C_{17}^r$. C_{15}^r is $1/N_c$ suppressed and therefore set to 0 in the resonance saturation model. C_{14}^r and C_{17}^r also do not get contributions from the resonances we included. In other models [14] C_{14}^r and C_{17}^r are estimated to be negative, but are very small in absolute value. In [14] the other L_i^r, appearing at NNLO in F_K/F_π, are set to the values of fit 10 [9]. The results of the fit to lattice data are quoted in the first column of Table 13. For comparison we quote in the same table the values as obtained by our best fits, including those for the random C_i^r search described in Section 7 and quoted in Table 18 in the appendix. The table shows that the value of L_5^r in fit All is compatible with the result of [14] within uncertanties and even more compatible when we look at the fit F_K/F_π in Table 5 where we required $L_4^r = 0$ as in [14]. The fits best reso and best rand instead are very different. For these last two fits we can also compare the values of the C_i^r-combinations. As far as regards the combination $C_{14}^r + C_{15}^r$ our random sets acquire both a negative value in contrast with [14]. The second combination instead agrees upon the sign, but are rather different in value.

For further comparison we can do also a fit similar to fit All but setting in addition $10^5 C_{14}^r = 0.31$ and $10^5 C_{17}^r = 0.55$. The results are given in Table 14.

The fit obtained is different from fit All, in particular we find an even lower L_5^r and the χ^2 is somewhat larger. The value of L_5^r has decreased quite a bit while the others are compatible with fit All but the central values for L_4^r and L_6^r are rather large. Finally notice that the L_i^r of fit All are very different from the ones of fit 10 and might therefore affect the findings of [14]. We cannot draw any further conclusions at present. In future work we intend to include more lattice results which should clarify this issue.

	$C_i^r[14]$
$10^3 L_1^r$	0.88 ± 0.09
$10^3 L_2^r$	0.53 ± 0.21
$10^3 L_3^r$	-2.97 ± 0.43
$10^3 L_4^r$	0.89 ± 0.83
$10^3 L_5^r$	0.30 ± 0.09
$10^3 L_6^r$	0.39 ± 0.97
$10^3 L_7^r$	-0.02 ± 0.16
$10^3 L_8^r$	0.13 ± 0.20
χ^2 (dof)	2.03 (4)

Table 14: The fit as obtained using the same input as fit All and the C_i^r as in the resonance estimate of Table 18 with the exception of C_{14}^r and C_{17}^r set respectively to 0.31×10^{-5} and 0.55×10^{-5}. The L_i^r are given at $\mu = 0.77$ GeV.

7 Releasing the C_i^r

All the fits presented in the previous section have unusual NNLO corrections to the masses and many also to the decay constants. In addition, if we included the requirement that the $\bar{\ell}_i$ were also fitted well we could not find a simple good fit.

An additional reason to go beyond what we have is that all the estimates used above with the exception of the singlet η contribution only contribute to the NNLO LECs[5] that are leading in N_c. In the masses and decay constants in addition the estimates from the resonance exchange give no contribution at leading order in N_c at all. This is an unsatisfying situation, we do expect that the masses and decay constants should get some contribution from the NNLO constants. Inspection of the relations between the $\bar{\ell}_i$ and the $SU(3)$ LECs [46] shows that only combinations of the C_i^r appear that are suppressed by N_c. Thus especially the problem with $\bar{\ell}_2$ above requires some nonzero values for the N_c suppressed constants.

We could in principle allow all the C_i^r to be free and include them in the fit as well. However, from our earlier work in [6] it is clear that with the inputs used at present there are enough free combinations of the C_i^r to fit all physical inputs directly. For this reason we also have explored another technique of C_i^r estimate, based on a random walk[6] method. Hereafter we describe the main features of the algorithm used. See also the flowchart in Figure 1. The algorithm is a version of simulated annealing.

We first start with an initial set $C_i^{r(\mathrm{in})} = C_i^{r(\mathrm{old})}$. These are chosen to be

1. random (with a size given by $1/3/(16\pi^2)^2$ for those leading in $1/N_c$ and $1/3$ of that for the subleading ones),

[5]This is true with the exception of terms involving $\langle \chi_- \rangle$ which can get produced by the equations of motion.

[6]The idea was born thanks to a discussion with Juerg Gasser and Gerhard Ecker.

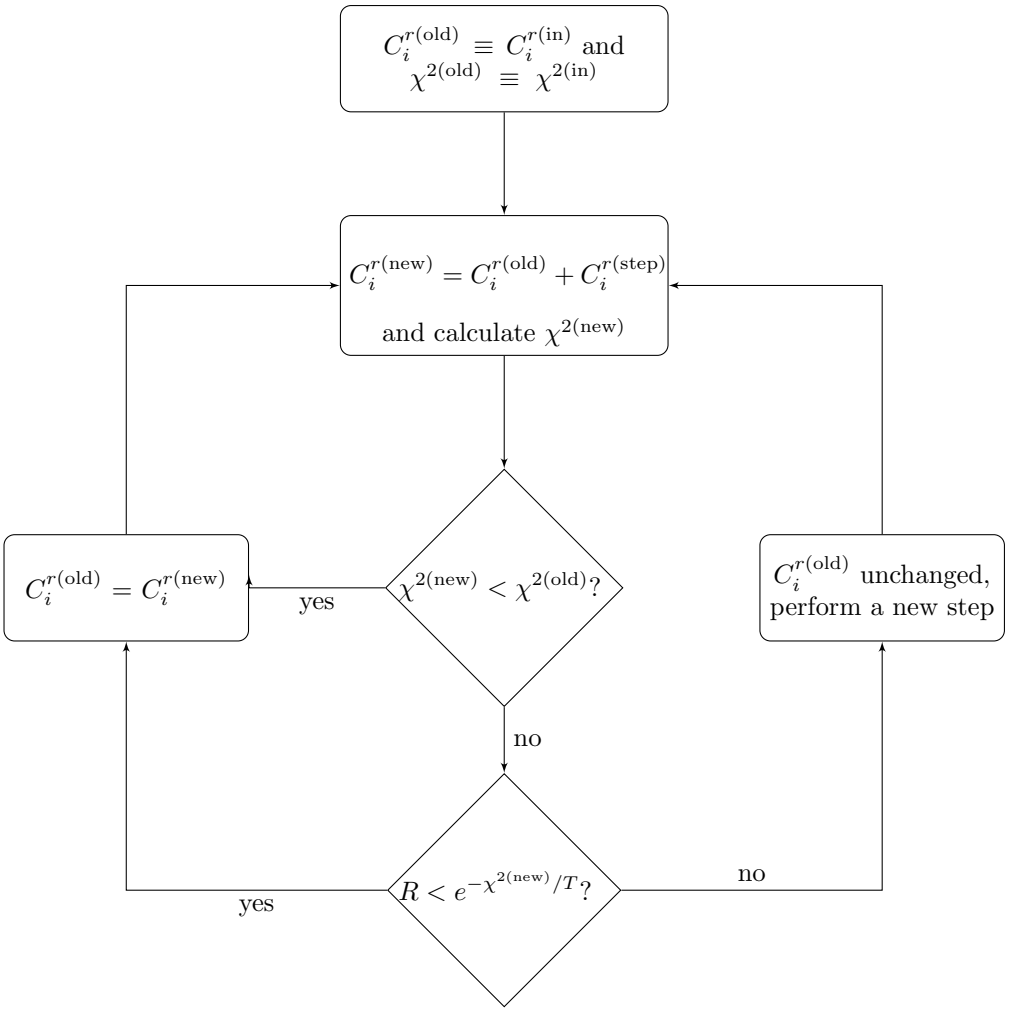

Figure 1: Algorithm used to select the random C_i^r. It has been started with different values of the initial $C_i^{r(\mathrm{in})}$, as explained in the text. In the bottom decision square R is a random number selected with a uniform distribution in the interval (0,1), while T is a parameter set such that it is of the same order of magnitude of the χ^2. More details can be found in the text.

2. all zero

3. as obtained by resonance estimate (see Table 18)

4. as obtained by multiplying the constants of [13] by 0.27 (see Table 18).

Then we perform the fit on the L_i^r using those $C_i^{r(\mathrm{old})}$. After this we take a random step according to the formula

$$C_i^{r(\mathrm{new})} = C_i^{r(\mathrm{old})} + C_i^{r(\mathrm{step})} \equiv C_i^{r(\mathrm{old})} + \frac{1}{(16\pi^2)^2}\epsilon r_i\,, \tag{42}$$

where r_i in (42) is a random number generated through a uniform distribution in the interval $(-1,1)$ and we have used $\epsilon = 0.01$ and 0.001. For those C_i^r that are N_c suppressed we further multiply $C_i^{r(\mathrm{step})}$ by 1/3. In this way the random generated C_i^r set still respects the large-N_c suppressions to a certain extent. We perform the fit of the L_i^r using the new set $C_i^{r(\mathrm{new})}$ and we check the χ^2 obtained. If the χ^2 decreases then we substitute the $C_i^{r(\mathrm{old})}$ with $C_i^{r(\mathrm{new})}$. Sometimes we also allow $C_i^{r(\mathrm{new})}$ to be selected even though the corresponding χ^2 is not smaller than the previous one (see last step in the flow diagram of Figure 1). This is done so to let the C_i^r to take quite different values and thus to test as many different sets as possible. It is also needed for our algorithm to be able to move out of local minima. We find that, when we let our algorithm run long enough, we cover quite many different sets of C_i^r. We chose different initial C_i^r to widen their range of variability. In addition we have started the random walk from the same starting point several times including different random starting points. We chose as random starting points $1/3/(16\pi^2)^2$ with the extra factor of 1/3 since without the extra 1/3 we never reached a χ^2 smaller than one.

The fits are performed including the same input as for fit All but with a few extra requirements. We add as input the curvature of the scalar formfactor c_S^π in (30) and all the $\bar{\ell}_i$ of the last column of Table 8. We do not instead demand to fit all the $\pi\pi$ and πK scattering parameters, since it costs in terms of computing time. So, as done for fit All, we include only a_0^0, a_2^0, $a_0^{1/2}$ and $a_0^{3/2}$. Notice that we do not find any large discrepancies when we add more scattering parameters in fit All, as was remarked at the end of Section 6.

We also require a good convergence of the masses and decay constants expansions. The reason is that in this way we have the possibility to "select" those C_i^r granting us convergence for those quantities. This also allows to keep under control the quality of the fits. Otherwise too much freedom would be left to the C_i^r constants, and many different fits with a low χ^2 but with very bad convergences, can be reached. Clearly such convergence constraints have a strong effect on the L_i^r constants as described in the next Section 7.1.

7.1 Convergence constraints

We devote this section to a discussion of the convergence constraints imposed on the masses and decay constants in the fits with random C_i^r. Let us first show the case of the decay constants.

We performed the fits constraining the NNLO contributions to F_π, F_K and F_K/F_π constants to be small, i.e. less than the 10% of the LO ones. Remember that the expansions for the F_π and F_K decay constants are

$$\begin{aligned} F_K &= F_0 + F_K|_{p^4} + F_K|_{p^6}\,, \\ F_\pi &= F_0 + F_\pi|_{p^4} + F_\pi|_{p^6}\,, \end{aligned} \tag{43}$$

and that in our fits, as explained in Section 3.2, we include their ratio as

$$\frac{F_K}{F_\pi} \approx 1 + \underbrace{\frac{F_K}{F_0}\bigg|_{p^4} - \frac{F_\pi}{F_0}\bigg|_{p^4}}_{\text{NLO}} \underbrace{+ \frac{F_K}{F_0}\bigg|_{p^6} - \frac{F_\pi}{F_0}\bigg|_{p^6} - \frac{F_K}{F_0}\bigg|_{p^4}\frac{F_\pi}{F_0}\bigg|_{p^4} + \frac{F_\pi}{F_0}\bigg|_{p^4}^2}_{\text{NNLO}}\,. \tag{44}$$

Specifically the convergence constraints are included through the following partial $\chi^2_{i(\text{part})}$:

$$\begin{aligned} \chi^2_{i(\text{part})} &= \left(\frac{F_\pi}{F_0}\bigg|_{p^6}/0.05\right)^2, \qquad \chi^2_{i(\text{part})} = \left(\frac{F_K}{F_0}\bigg|_{p^6}/0.05\right)^2, \\ \chi^2_{i(\text{part})} &= \left(\frac{F_K}{F_\pi}\bigg|_{\text{NNLO}}/0.07\right)^2, \end{aligned} \tag{45}$$

With (45) we have been able to find many fits with a good convergence. On the other hand the NLO contribution for F_π turns out to be smaller than the expected 30%. The reason resides in the third of the relations in (45). Requiring all the NNLO pieces for all the decay constants to be small implies that the single contributions $F_\pi|_{p^6}$ and $F_K|_{p^6}$ are small. But also the term $(F_\pi/F_0)|^2_{p^4}$ must be small, otherwise the NNLO contribution of F_K/F_π is allowed to be large. This leads to small NLO corrections for F_π and thus a $F_0 \approx F_\pi$.

We apply similar restrictions also to the masses

$$\chi^2_{i(\text{part})} = \left(\frac{m^2_M}{m^2_{M\,0}}\bigg|_{p^6}/0.1\right)^2 \tag{46}$$

where M stands for π, K and η mesons and $m_{M\,0}$ are the leading order contributions to the masses. We have kept the value of $m_s/\hat{m}$ fixed at 27.8 as for fit All.

We conclude this section with a final remark. One might wonder why we have not imposed similar constraints also for fit All, since these could improve the convergence of the expansions. The reason is that when we require them, we obtain a reasonably good fit ($\chi^2 \approx 8$ with 10 degrees of freedom) and with better constrained L^r_4 and L^r_6. But it also causes much worse predictions for the $\bar{\ell}_i$, e.g. $\bar{\ell}_3 \approx 6.5$.

7.2 Results

Now we are ready to show the outcomes of our studies when the C^r_i are set to random values using the procedure of Figure 1 and with the constraints listed in Section 7.1 above.

$C_i^{r(\mathrm{in})}$	resonance	zero	CQM	random
$10^3 L_1^r$	$(0.6, 1.2)$	$(0.5, 1.1)$	$(0.2, 0.6)$	$(0.3, 1.2)$
$10^3 L_2^r$	$(0.4, 1.2)$	$(0.2, 0.8)$	$(-0.2, 0.5)$	$(0, 1.6)$
$10^3 L_3^r$	$(-5.5, -3.0)$	$(-4.5, -3.0)$	$(-3.3, -1.2)$	$(-6.2, -2.0)$
$10^3 L_4^r$	$(0.15, 0.35)$	$(-0.1, 0.25)$	$(-0.1, 0.2)$	$(0.05, 0.35)$
$10^3 L_5^r$	$(1.2, 1.6)$	$(1.35, 1.5)$	$(1.25, 1.55)$	$(1.2, 1.6)$
$10^3 L_6^r$	$(-0.05, 0.25)$	$(-0.2, 0.2)$	$(-0.15, 0.15)$	$(-0.05, 0.3)$
$10^3 L_7^r$	$(-0.45, -0.1)$	$(-0.43, -0.18)$	$(-0.43, -0.24)$	$(-0.45 - 0.2)$
$10^3 L_8^r$	$(0.4, 0.8)$	$(0.45, 0.72)$	$(0.5, 0.731)$	$(0.45, 75)$

Table 15: The ranges for L_i^r values as obtained changing the C_i^r according to a random walk algorithm. The different ranges correspond to different initial values for the C_i^r. With CQM we indicate the C_i^r of the chiral quark model. All the fits have a $\chi^2 < 1$. For all the fits $\mu = 0.77$ GeV. See the description in the text for further details on how the fits have been performed.

First of all we must point out that due to the freedom we allow to the C_i^r many different fits of the L_i^r have a low χ^2. We set initial C_i^r equal to zero, resonance exchange or chiral quark model estimates as well more random starts. We easily reach $\chi^2 < 1$, and we found many fits with $\chi^2 \approx 0.5$. Reducing the steps of the random walk we can even find smaller values. However once the χ^2 reaches a reasonably low value, e.g. 1, there is no apparent reason why one should prefer one specific fit to another. Due to the several different sets of C_i^r under study, we can only quote the ranges where the L_i^r vary and where we obtain a $\chi^2 < 1$. Such ranges are quoted in Table 15 and are obtained, starting from different initial sets $C_i^{r(\mathrm{in})}$. Keep in mind that these ranges depend on the C_i^r chosen. Plugging in a L_i^r fit without the corresponding C_i^r will not produce any sensible results. The way we determined those numbers is shown in Figure 2 on the example for L_1^r where we have plotted a number of fits that gave $\chi^2 < 1$ for the different starting points. We have typically stopped the fits when a χ^2 of about 0.4 or below was found and the tails at low χ^2 are an artefact, they were done with runs with a very low ϵ and a very low T.

The results are rather cumbersome. L_1^r, L_2^r and L_3^r look quite free to vary in large ranges. Notice also that the large N_c relation $2L_1^r \approx L_2^r$ is still not recovered. On the other hand, due to the converge constraints of Section 7.1 we narrow the intervals for the other constants. Especially L_5^r takes a large value and L_4^r a small one. As explained in Section 7.1, we essentially require that F_K/F_π, F_K and F_π have small NNLO corrections which give that F_K/F_π is given by the NLO and thus determines L_5^r at a fairly large value. That F_π has small corrections at all then in turn requires a fairly small L_4^r. The choice to constrain the convergence of those quantities is dictated by the lack of information to constrain more the C_i^r. When we release such constraints indeed we find different looking fits, but affected by a bad convergence. Somewhat more surprising is that the L_6^r typically takes on values that are smaller than L_8^r.

As you can see no clear final conclusion can be drawn with such results. When we

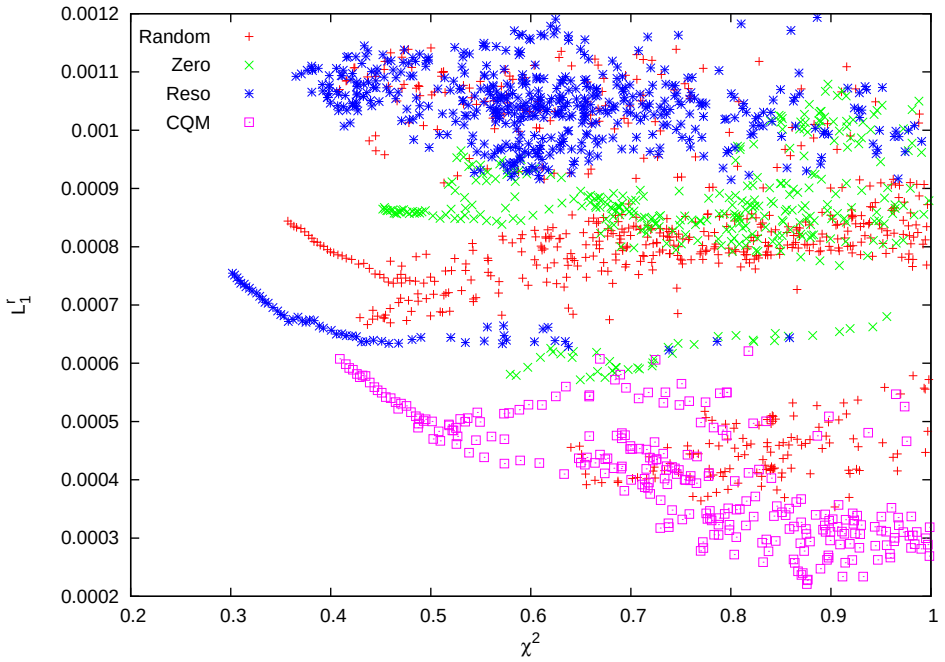

Figure 2: The values of L_1^r for the random walk fits of Table 15. In the plot all the fits are collected. The ranges of variability for L_1^r is quite large. In the picture it is also evident how the two values of the couplings depend somwehat on the different initial values of the C_i^r constants. The L_i^r are at the scale $\mu = 0.77$ GeV.

C_i^r	best reso	best random
$10^3 L_1^r$	0.75 ± 0.09	0.85 ± 0.09
$10^3 L_2^r$	0.81 ± 0.45	0.54 ± 0.05
$10^3 L_3^r$	-3.91 ± 0.28	-3.51 ± 0.28
$10^3 L_4^r$	0.16 ± 0.10	0.20 ± 0.10
$10^3 L_5^r$	1.40 ± 0.09	1.40 ± 0.09
$10^3 L_6^r$	0.10 ± 0.14	0.12 ± 0.14
$10^3 L_7^r$	-0.32 ± 0.13	-0.32 ± 0.13
$10^3 L_8^r$	0.64 ± 0.16	0.63 ± 0.16
χ^2	0.30	0.36

Table 16: The results as obtained using the C_i^r from the best χ^2 found starting from the resonance or from a completely random one as described in the text. The L_i^r are given at $\mu = 0.77$ GeV. The corresponding C_i^r sets can be found in Table 18 in appendix.

C_i^r	best reso			best random		
	p^2	p^4	p^6	p^2	p^4	p^6
m_π^2	0.987	0.021	-0.008	0.993	0.021	-0.012
m_K^2	1.057	-0.054	-0.003	1.060	-0.058	-0.002
m_η^2	1.132	-0.133	0.001	1.136	-0.135	-0.001
F_π/F_0	1	0.178	-0.010	1	0.187	-0.010
F_K/F_0	1	0.395	0.009	1	0.404	0.011
F_K/F_π	1	0.217	-0.020	1	0.217	-0.020

Table 17: The convergence for the best χ^2 found starting from the resonance estimate, here $F_0 = 0.079$ GeV. Fit as in left column of Table 16. The convergence for the best χ^2 found starting from the fully random estimate, here $F_0 = 0.078$ GeV. Fit as in left column of Table 16.

performed this study we were hoping not to find as many good fits and smaller ranges for the L_i^r. The study shows instead that it is very difficult, if not impossible, to narrow the ranges for the L_i^r with such a poor knowledge of the C_i^r. On the other hand it also shows that fits of the L_i^r with good convergence do exist, if the C_i^r are changed. In Table 16 we show the L_i^r obtained for the smallest χ^2 found starting from the resonance estimate and from fully random C_i^r as described above and we show the convergence for some quantities in those two fits in Table 17. The fits with very low χ^2 we have obtained, such as the two shown here, tend to have similar expansions for the masses and the decay constants. In order to see how the various C_i^r look like we have added the values for these two fits in the appendix.

We can draw some conclusions by studying correlations. The effect of $\bar{\ell}_2$ is very visible if we plot for the various fits with $\chi^2 < 1$ L_2^r, which is the NLO dependence of $\bar{\ell}_2$ on the LECs,

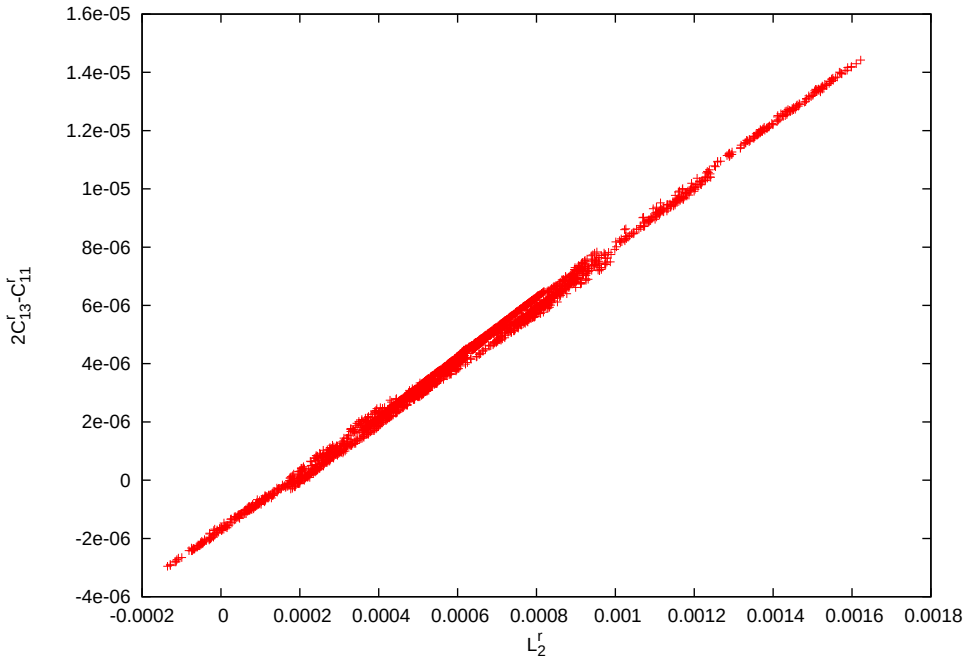

Figure 3: The correlations between L_2^r and $2C_{13}^r - C_{11}^r$. This results from including the value of $\bar{\ell}_2$ in the fit.

versus $2C_{13}^r - C_{11}^r$, which is the dependence on the NNLO LECs. The tight correlation shows that the NNLO contribution depends very little on the other L_i^r. More precisely, this shows the NLO LEC combination at NLO versus the NNLO LEC combination at NNLO and that the NNLO contribution depends fairly little on the value of the L_i^r. We get more of those constraints directly. A very similar one is from the value of $\bar{\ell}_1$ shown in Figure 4. The correlations for other observables tend to be weaker indicating that the NNLO contributions are more dependent on the value of the L_i^r for these cases. We show examples with a weaker but still existing correlation in Figure 5 where the correlations resulting from F_K/F_π are shown and in Figure 6 for $\langle r^2\rangle_S^\pi$. In both cases we have plotted on the horizontal axis the combination of L_i^r the quantity depends on at NLO and on the vertical axis the combination of C_i^r the quantity depends on at NNLO.

There are also correlation between the fitted values of the L_i^r. L_1^r, L_2^r and L_3^r show a reasonable correlation among themselves but are essentially not correlated with the others. There are weaker correlations between L_4^r and L_6^r and between L_7^r and L_8^r. These correlations are shown in Figures 7, 8, 9, 10, and 11. We have shown a curve in all plots guiding the eye as well and given it in the caption of the figure.

Note that throughout this section we have considered all fits with a $\chi^2 < 1$ to be essentially possible.

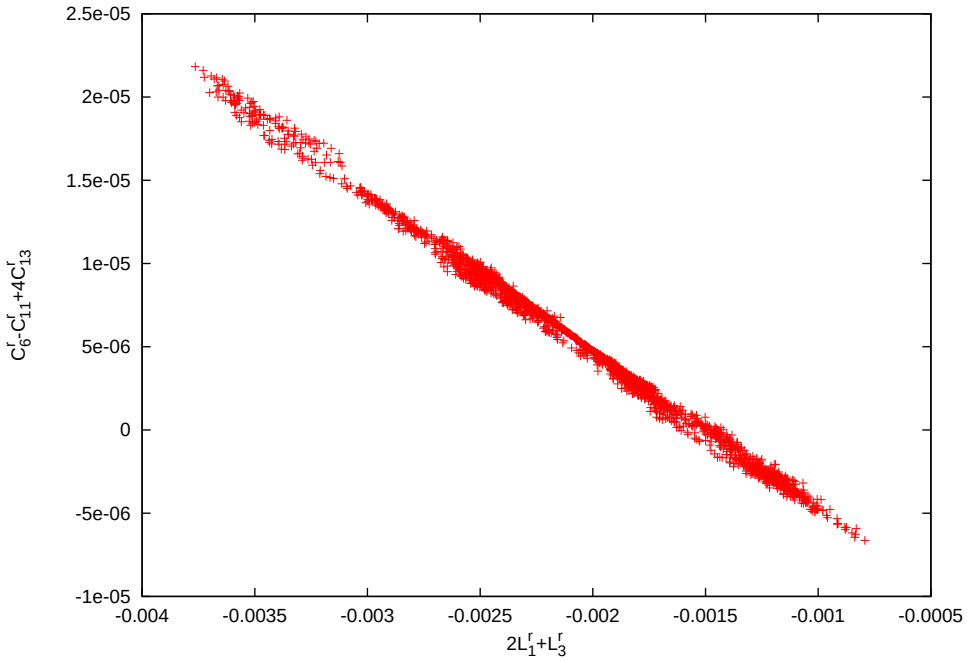

Figure 4: The correlations between $2L_1^r + L_3^r$ and $C_6^r - C_{11}^r + 4C_{13}^r$. This results from including the value of $\bar{\ell}_1$ in the fit.

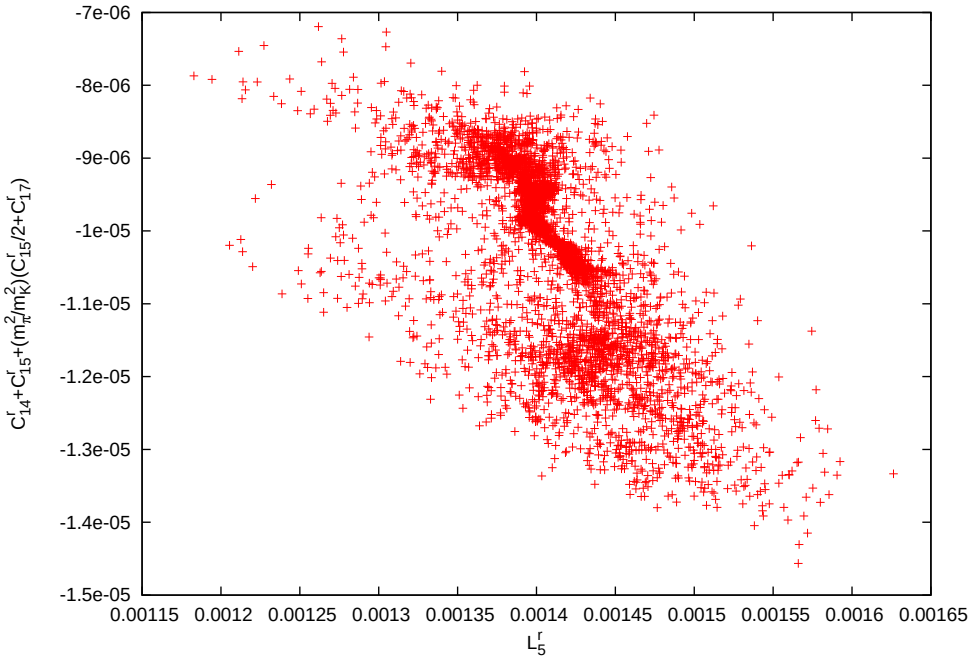

Figure 5: The correlations resulting from F_K/F_π.

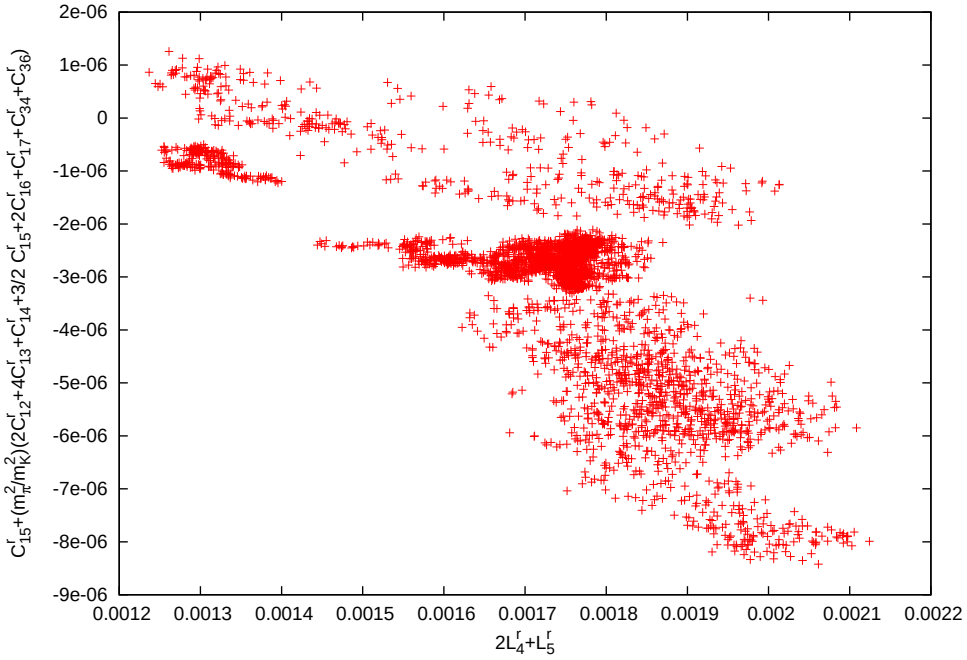

Figure 6: The correlations resulting from the pion scalar radius $\langle r^2\rangle_S^\pi$.

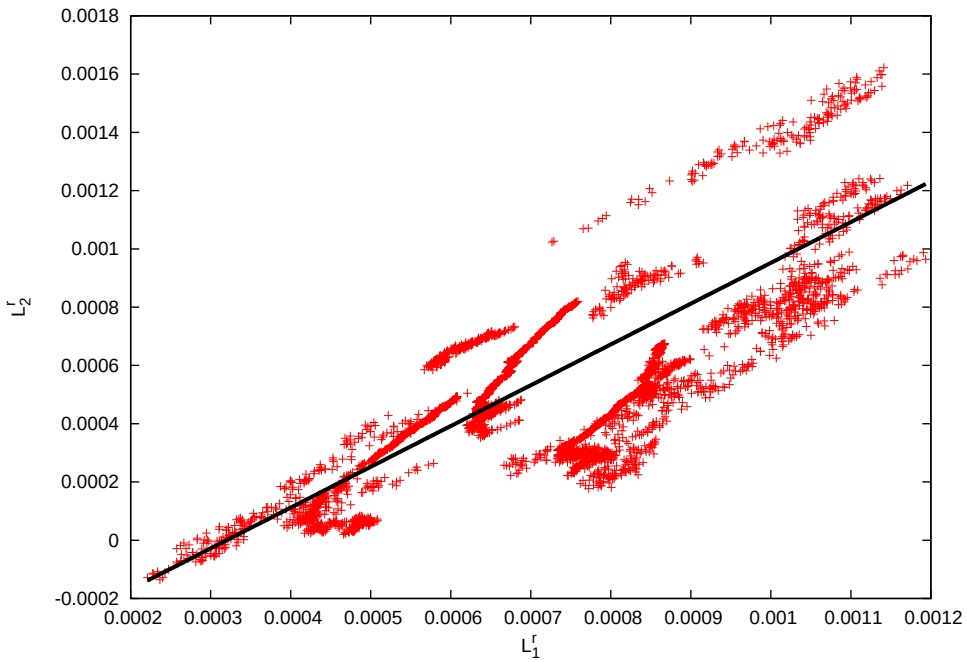

Figure 7: The correlations between L_1^r and L_2^r, the curve shown is $L_2^r = 1.4(L_1^r - 0.00032)$.

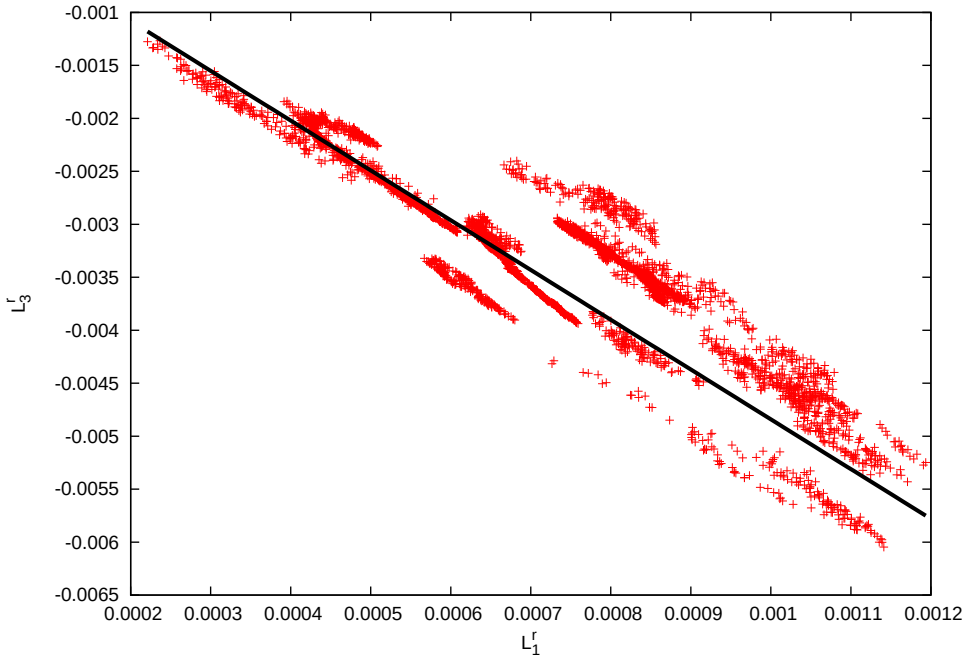

Figure 8: The correlations between L_1^r and L_3^r, the curve shown is $L_3^r = -4.7(L_1^r + 0.00003)$.

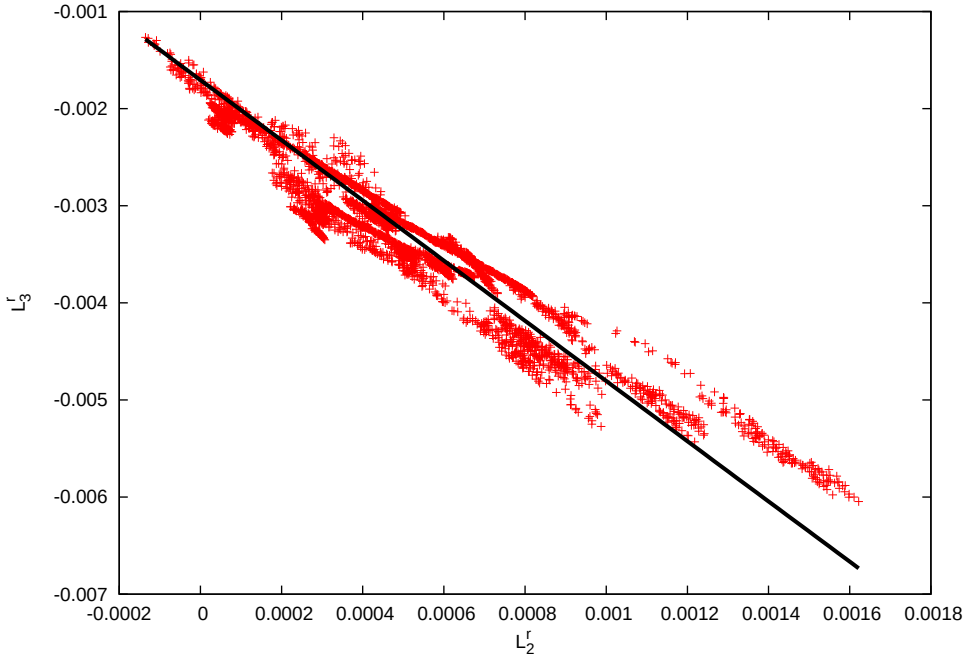

Figure 9: The correlations between L_2^r and L_3^r, the curve shown is $L_3^r = -3.1(L_2^r + 0.00055)$.

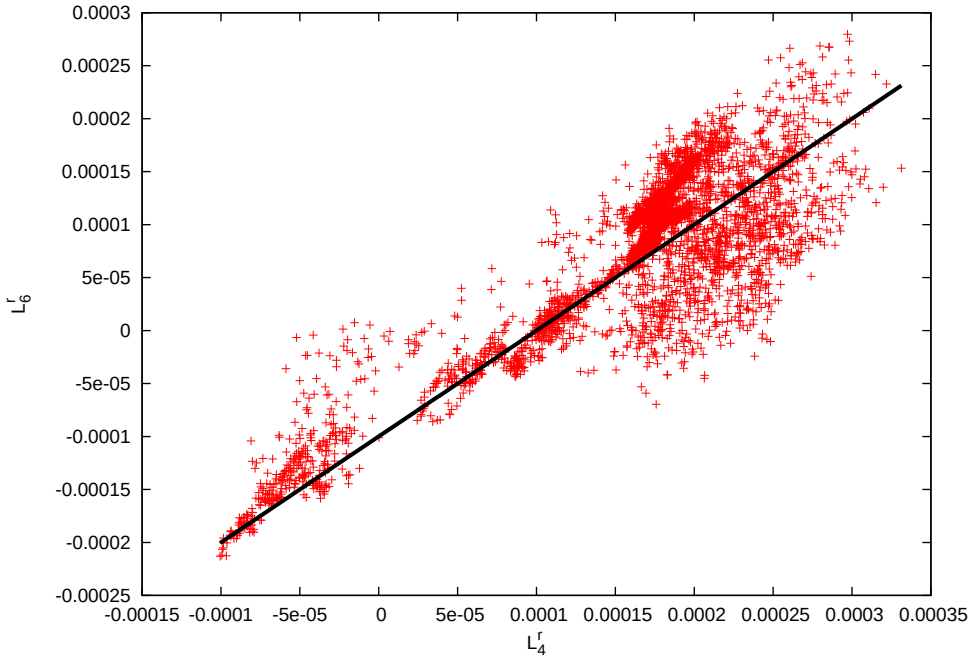

Figure 10: The correlations between L_4^r and L_6^r, the curve shown is $L_6^r = L_4^r - 0.0001$.

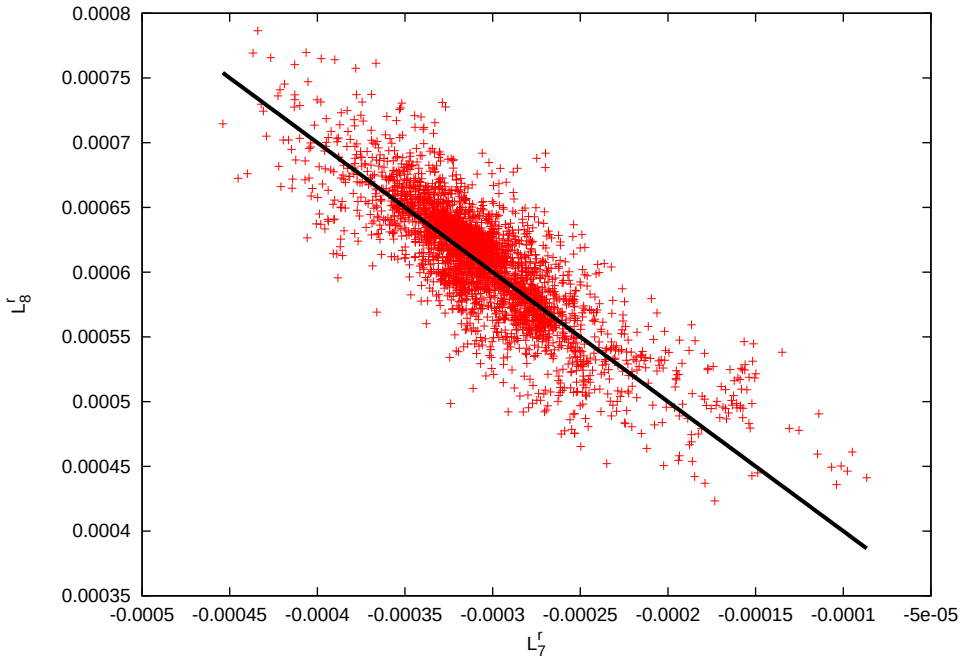

Figure 11: The correlations between L_7^r and L_8^r, the curve shown is $L_8^r = -(L_7^r - 0.0003)$.

8 Conclusions

In this paper we have shown the results for a new global fit of the L_i^r at NNLO, with techniques similar to the ones in [8, 9]. Different treatments of the p^6 coupling constants have been considered: the resonance estimate of [8], the results of [13] and the use of randomly selected C_i^r. The results are difficult to interpret and unexpected. All the fits that have been performed using the NNLO couplings from [8] or [13] show both strong and weak points. The fits obtained from the randomly selected C_i^r are too different from each other to draw a final conclusion, although they give a rough indication on where we can expect to find the values of L_i^r. They also provide a proof of principle that with reasonable values of the C_i^r a reasonably convergent series for $SU(3)$ ChPT can be obtained for many quantities.

The fit that presents the least discrepancies and best convergence of the chiral expansion is fit All in Table 5, which has been obtained with the resonance estimate of the C_i^r. It succeeds in fitting many observables like the $\pi\pi$ and πK scattering parameters and the slope of the scalar formfactor of the pion. It also reproduces quite well the experimental results for the f_s and g_p $K_{\ell 4}$ formfactors although it does not predict the curvature of f_s. The perturbative expansions for masses and decay constants reported in (36) and (37) look suspicious but are acceptable. On the other hand it does not satisfy the large N_c relation $2L_1^r \approx L_2^r$ and it fails in well constraining the L_4^r and L_6^r values. Finally its prediction for $\bar{\ell}_2$ is far from the current estimate of that constant. We have at present not included many results from lattice QCD. We expect that this should improve in a few years allowing for another step forward in confronting ChPT with data.

Acknowledgments

We thank Juerg Gasser, Gerhard Ecker, Veronique Bernard, Emilie Passemar, Antonio Pich and Gilberto Colangelo for discussions. This work is supported in part by the European Community-Research Infrastructure Integrating Activity "Study of Strongly Interacting Matter" (HadronPhysics2, Grant Agreement n. 227431) and the Swedish Research Council grants 621-2008-4074 and 621-2010-3326.

A C_i values

The aim of this section is to present the values used for the C_i^r. We only present results for the C_i^r that actually contribute to the observables we have included in the fits and we indicate with the superscript $*$ the ones that are subleading in N_c. They can all be found in Table 18 The column labelled reso is the resonance exchange estimate of Section 4. The column labelled CQM is the estimate of [13] as discussed in Section 6.4. The values directly from their model can be found in Table IV of [13]. The values in the column labelled CQM have been multiplied with nomalization factor $\alpha = 0.27$ from the fit in the right column of Table 9. The normalization from the fit to the linear NA48/2 input,

Table 11 is a little smaller but essentially the same. The last two columns are from the random walk/simulated annealing estimates for the C_i^r reported in Section 7 from the best χ^2 found starting from the resonance estimate and a fully random starting point. These are the C_i^r for the fits reported in Table 16.

The main purpose is to show the typical sizes of the C_i^r we obtained for the fits and that the pattern for the good fits can be quite different.

References

[1] S. Weinberg, Physica **A96** (1979) 327.

[2] J. Gasser and H. Leutwyler, Annals Phys. **158** (1984) 142.

[3] J. Gasser and H. Leutwyler, Nucl. Phys. B **250** (1985) 465.

[4] J. Bijnens, G. Colangelo, G. Ecker, JHEP **9902** (1999) 020. [hep-ph/9902437].

[5] J. Bijnens, Prog. Part. Nucl. Phys. **58** (2007) 521 [hep-ph/0604043].

[6] J. Bijnens, I. Jemos, Eur. Phys. J. **C64** (2009) 273-282. [arXiv:0906.3118 [hep-ph]].

[7] J. Bijnens, G. Colangelo, J. Gasser, Nucl. Phys. **B427** (1994) 427-454. [hep-ph/9403390].

[8] G. Amorós, J. Bijnens and P. Talavera, *Nucl. Phys.* B **585** (2000) 293 [Erratum-ibid. B **598** (2001) 665] [hep-ph/0003258].

[9] G. Amorós, J. Bijnens and P. Talavera, *Nucl. Phys.* B **602** (2001) 87 [hep-ph/0101127].

[10] J. Bijnens, P. Dhonte, JHEP **0310** (2003) 061. [hep-ph/0307044].

[11] J. Bijnens, P. Dhonte, P. Talavera, JHEP **0401** (2004) 050. [hep-ph/0401039].

[12] J. Bijnens, P. Dhonte and P. Talavera, *J. High Energy Phys.* **0405** (2004) 036 [hep-ph/0404150].

[13] S. -Z. Jiang, Y. Zhang, C. Li *et al.*, Phys. Rev. **D81** (2010) 014001. [arXiv:0907.5229 [hep-ph]].

[14] G. Ecker, P. Masjuan, H. Neufeld, Phys. Lett. **B692** (2010) 184-188. [arXiv:1004.3422 [hep-ph]].

[15] A. Pich, Lectures at Les Houches Summer School in Theoretical Physics, Session 68: Probing the Standard Model of Particle Interactions, Les Houches, France, 28 Jul - 5 Sep 1997, [hep-ph/9806303].

[16] S. Scherer, *Adv. Nucl. Phys.*, 27 (2002) 277 [hep-ph/0210398].

i	reso	CQM	best reso	best rand	i	reso	CQM	best reso	best rand
1	1.216	0.866	1.683	−0.733	25	−1.838	−1.366	−1.452	1.282
2*	0.000	0.000	0.113	0.280	26	−0.284	0.765	−0.597	−0.485
3	0.000	−0.011	0.324	0.084	27*	−0.261	−0.352	−0.228	−0.155
4	1.452	0.708	2.225	1.266	28*	0.135	0.069	0.177	0.147
5	0.619	−0.231	0.779	1.147	29	−1.363	−0.704	−1.907	−0.785
6*	0.000	0.000	−0.307	−0.050	30*	0.270	0.137	0.165	0.545
7*	0.000	0.000	0.350	−0.003	31	−0.616	−0.144	−0.389	1.310
8	0.619	0.528	1.434	0.615	32*	−0.002	0.041	0.291	0.356
9*	0.000	0.000	0.148	−0.194	33*	0.208	0.021	0.291	−0.102
10	−1.239	−0.240	−0.164	0.307	34	1.432	0.363	2.321	1.077
11*	0.000	0.000	−0.112	−0.344	35*	−0.009	0.039	0.236	0.146
12	−0.619	−0.078	−1.358	−0.512	36*	0.000	0.000	−0.169	−0.087
13*	0.000	0.000	0.265	−0.002	63	0.619	0.683	0.665	0.776
14	0.000	−0.190	−0.759	−0.828	64*	0.000	0.000	0.389	−0.095
15*	0.000	0.000	−0.228	−0.233	65	1.239	−0.555	0.611	0.432
16*	0.000	0.000	0.007	0.063	66	1.049	0.391	1.703	0.416
17	0.000	0.002	0.125	1.121	67*	0.000	0.000	−0.304	0.017
18*	−0.202	−0.128	−0.284	−0.063	68*	0.000	0.000	0.002	0.536
19	0.001	−0.110	−0.411	−1.147	69	−0.577	−0.196	−0.664	−0.784
20*	−0.002	0.041	−0.335	−0.043	83	0.163	0.016	−0.294	−0.553
21*	0.001	−0.014	0.018	−0.088	84*	0.000	0.000	0.357	−0.264
22	−0.297	0.062	0.545	1.117	88	−1.383	−1.249	−0.912	−0.331
23*	0.000	0.000	0.048	0.269	90	5.069	0.557	5.238	−0.204
24*	0.811	0.370	0.694	0.013					

Table 18: The C_i^r constants as obtained by several methods. In the table we quote $10^5 \times C_i^r$ were the i is given in the first column. The i^* indicates a N_c suppressed C_i^r. The second column corresponds to the resonance model of Section 4. In the third one we quote the C_i^r of [13] multiplied by $\alpha = 0.27$. The particular value of α is chosen fitting it to the input observables together with the L_i^r, as explained in Section 6.4. In the last two columns we quote two sets of C_i^r corresponding to the best fits of the L_i^r when the C_i^r are realesed, as explained in Section 7. The column labeled best reso comes from initial values of the C_i^r equal to the ones of the resonance estimate, while in the column labeled best rand even the initial values of the C_i^r are chosen randomly. The scale of renormalization for all the sets is $\mu = 0.77$ GeV.

[17] F. James, M. Roos, Comput. Phys. Commun. **10** (1975) 343-367.

[18] http://lcgapp.cern.ch/project/cls/work-packages/mathlibs/minuit/

[19] G. Amoros, J. Bijnens, P. Talavera, Nucl. Phys. **B568** (2000) 319-363. [hep-ph/9907264].

[20] Nakamura *et al.* [Particle Data Group Collaboration], J. Phys. G **G37** (2010) 075021.

[21] J. Bijnens, I. Jemos, PoS **CD09** (2009) 087. [arXiv:0909.4477 [hep-ph]].

[22] J. Bijnens, I. Jemos, PoS **EFT09** (2009) 032. [arXiv:0904.3705 [hep-ph]].

[23] C. Amsler *et al.* [Particle Data Group Collaboration], Phys. Lett. **B667** (2008) 1-1340.

[24] G. Colangelo, S. Durr, A. Juttner *et al.*, Eur. Phys. J. **C71** (2011) 1695. [arXiv:1011.4408 [hep-lat]].

[25] J. Bijnens, J. Prades, Nucl. Phys. **B490** (1997) 239-271. [hep-ph/9610360].

[26] G. Amorós and J. Bijnens, *J. Phys.* G **25** (1999) 1607 [hep-ph/9902463].

[27] L. Ametller, J. Bijnens, A. Bramon, F. Cornet, Phys. Lett. **B303** (1993) 140-146. [hep-ph/9302219].

[28] P. Truoel *et al* [E865 collaboration], [hep-ex/0012012].

[29] J. R. Batley *et al.* [NA48-2 Collaboration], Eur. Phys. J. **C70** (2010) 635-657.

[30] S. Pislak *et al.* [BNL-E865 Collaboration], Phys. Rev. Lett. **87** (2001) 221801. [hep-ex/0106071].

[31] G. Colangelo, J. Gasser and H. Leutwyler, *Nucl. Phys.* B **603** (2001) 125 [hep-ph/0103088].

[32] G. Colangelo, J. Gasser, A. Rusetsky, Eur. Phys. J. **C59** (2009) 777-793. [arXiv:0811.0775 [hep-ph]].

[33] P. Buettiker, S. Descotes-Genon and B. Moussallam, *Eur. Phys. J.* C **33** (2004) 409 [hep-ph/0310283].

[34] J. F. Donoghue, J. Gasser, H. Leutwyler, Nucl. Phys. **B343** (1990) 341-368.

[35] B. Moussallam, Eur. Phys. J. **C14** (2000) 111-122. [hep-ph/9909292].

[36] B. Ananthanarayan, I. Caprini, G. Colangelo, J. Gasser, H. Leutwyler, Phys. Lett. **B602** (2004) 218-225. [hep-ph/0409222].

[37] S. Aoki *et al.* [JLQCD and TWQCD Collaborations], Phys. Rev. **D80** (2009) 034508. [arXiv:0905.2465 [hep-lat]]

[38] J. Bijnens, P. Talavera, JHEP **0203** (2002) 046. [hep-ph/0203049].

[39] M. Gonzalez-Alonso, A. Pich, J. Prades, Phys. Rev. **D78** (2008) 116012. [arXiv:0810.0760 [hep-ph]].

[40] G. Ecker, J. Gasser, A. Pich, E. de Rafael, Nucl. Phys. **B321** (1989) 31

[41] J. F. Donoghue, C. Ramirez, G. Valencia, Phys. Rev. **D39** (1989) 1947.

[42] V. Cirigliano, G. Ecker, M. Eidemuller *et al.*, Nucl. Phys. **B753** (2006) 139-177. [hep-ph/0603205].

[43] K. Kampf, J. Novotny, J. Trnka, Eur. Phys. J. **C50** (2007) 385-403. [hep-ph/0608051].

[44] J. Bijnens, K. Ghorbani, JHEP **0711** (2007) 030. [arXiv:0709.0230 [hep-ph]].

[45] J. Bijnens, P. Talavera, Nucl. Phys. **B669** (2003) 341-362. [hep-ph/0303103].

[46] J. Gasser, C. Haefeli, M. A. Ivanov *et al.*, Phys. Lett. **B652** (2007) 21-26. [arXiv:0706.0955 [hep-ph]].

[47] J. Gasser, C. Haefeli, M. A. Ivanov *et al.*, Phys. Lett. **B675** (2009) 49-53. [arXiv:0903.0801 [hep-ph]].

[48] S. Durr, Z. Fodor, C. Hoelbling, S. D. Katz, S. Krieg, T. Kurth, L. Lellouch, T. Lippert *et al.*, Phys. Rev. **D81** (2010) 054507. [arXiv:1001.4692 [hep-lat]].